CoCrMo Alloy

in vitro and *in vivo* studies

PhD thesis

Stig Storgaard Jakobsen

Faculty of Health Sciences
University of Aarhus
2008

CoCrMo Alloy

in vitro and *in vivo* studies

PhD thesis

Stig Storgaard Jakobsen

Faculty of Health Sciences
University of Aarhus

The Department of Orthopedics,
University Hospital Aarhus,
Aarhus, Denmark

&

Neurobiology, Institute of Anatomy,
University of Aarhus,
Aarhus, Denmark

&

Department of Endocrinology and Metabolism C,
University Hospital Aarhus
Aarhus, Denmark

Correspondence:

Stig Storgaard Jakobsen, M.D.
Department of Orthopedics
Aarhus University Hospital
Tage-Hansens Gade 2, Building 10A
DK-8000 Aarhus C
Denmark
Phone +45 4097 6165
E-mail: StigSJ@dadlnet.dk
www.OrthoResearch.dk

List of papers

I **Cobalt - Chromium - Molybdenum Alloy Causes Metal Accumulation and Metallothionein Upregulation in Rat Liver and Kidney**
Stig S. Jakobsen, Gorm Danscher, Meredin Stoltenberg, Agnete Larsen, Jens M. Bruun, Tina Mygind, Kaare Kemp, Kjeld Soballe – Basic Clin Pharmacol Toxicol. 2007 Dec;101(6):441-6.

II **Effects of As-cast and Wrought Cobalt-Chrome-Molybdenum and Titanium-Aluminium-Vanadium Alloys on Cytokine Gene Expression and Protein Secretion in J774A.1 Macrophages**
Stig S. Jakobsen, Agnete Larsen, Meredin Stoltenberg, Jens M. Bruun, Kjeld Søballe – Eur Cell Mater. 2007 Sep 11;14:45-54; discussion 54-5

III **Hydroxyapatite coatings did not increase TGF-β and BMP-2 secretion in murine J774A.1 macrophages, but induced pro-inflammatory cytokine response**
Stig S. Jakobsen, Agnete Larsen, Meredin Stoltenberg, Jens M. Bruun, Kjeld Soballe – Accepted for publication in Journal of Biomaterials Science: Polymer Edition 2008

IV **CoCrMo PoroCoat® Mechanical Implant Fixation Inferior to Titanium PoroCoat® in a Canine Implant Model**
Stig S. Jakobsen, Jorgen Baas, Thomas Jakobsen, Kjeld Soballe – Submitted to Biomaterials 2008

Preface

This thesis is submitted to the Faculty of Health Science at the University of Aarhus as a part of the requirements for the Ph.D. – degree in Medical Science.

I am greatly indebted to my enthusiastic and patient supervisors Professor Kjeld Søballe MD., D.M.Sc., Jens Meldgaard Bruun MD., Ph.D., and Meredin Stoltenberg MD., D.M.Sc. Your support has always been invaluable.

Jørgen Baas MD., Ph.D. student, Agnete Larsen MD., Ph.D., Thomas Jakobsen MD., Ph.D. Student., Thomas Baad-Hansen MD., Ph.D., and Maiken Stilling MD., Ph.D. Student all helped me tremendously and we had many fruitful conversations.
Niels Trolle Andersen, Lic. Scient, Department of Biostatistics is thanked for valuable guidance with statistics and Professor Gorm Danscher D.M.Sc. for enthusiastic discussions and his valuable advices. I am also grateful to Ms. Lene Munkøe, Ms. Dorete Jensen, Ms. Janne Svejstrup (Neurobiology, Institute of Anatomy), Ms. Pia Hornbek, Ms. Lenette Pedersen (Department of Endocrinology and Metabolism C) and Ms. Anette Baatrup, Ms. Anna Bay Nielsen, Ms. Jane Pauli, and Ms. Annette Milton (Department of Orthopedics) for their skilful technical and linguistically assistance.

Finally, I would like to thank the three persons that mean the most to me, my best friend and loving wife Lotte Kaasgaard Jakobsen, and our two wonderful kids, Thøger and Hanne.

Acknowledgements

I received generous financial support from The Danish Rheumatic Society, and Århus Universitetshospitals Forskningsinitiativ, A.P. Møller og Hustru Chasmines fond til almene formaal, The Korning foundation, and The Lundbeck foundation.
Biomet Inc., Warsaw, IN, USA kindly donated the CoCrMo discs and the plasmaspray discs. Smith & Nephew Orthopedics, Inc., Memphis, TN, USA kindly donated the porous coated discs. CoCrMo wire was kindly donated by Fort Wayne Metals, Research Products Corp. Indiana, USA. DePuy Orthopedics Inc. donated the implants for study IV and supported the study financially.

Abbreviations

IL-1α	Interleukin-1 alpha
IL-1β	Interleukin-1 beta
IL-6	Interleukin-6
IL-10	Interleukin-10
MCP-1	Monocyte chemoattractant protein-1
MIP-1α	Macrophage inflammatory protein-1alpha
M-CSF	Macrophage Colony-Stimulation Factor
OPG	Osteoprotegerin
TGF-β	Transforming growth factor beta
TNF-α	Tumor necrosis factor-alpha
BMP-2	Bone morphogenetic protein-2
RANTES	Regulated upon Activation, Normal T-cell Expressed, and Secreted
RANK	Receptor Activator of Nuclear factor kappa Beta
RANKL	Receptor Activator of Nuclear factor kappa Beta ligand
HA	Hydroxyapatite
CoCrMo	Cobalt-Chromium-Molybdenum alloy
TiAlV	Titanium-Aluminium-Vanadium alloy
PIXE	Proton Induced X-ray Emission

Definitions

Biocompatibility:	The ability of a material to perform with an appropriate host response in a specific application.
Commercial 3D-surface:	Porous structure coatings on commercial available joint replacement implants.
Alloy:	An alloy is a homogeneous mixture of two or more elements, at least one of which is a metal, and where the resulting material has metallic properties. The resulting metallic substance usually has different properties (sometimes substantially different) from those of its components.
Cast:	Casting is a manufacturing process by which a liquid material such as a suspension of molten metal or plastic is introduced into a mould, allowed to solidify within the mould, and then ejected or broken out to make a fabricated part. Casting is used for making parts of complex shape that would be difficult or uneconomical to make by other methods, such as cutting from solid material.
Wrought:	Wrought material has been heated and shaped using localised compressive forces (forged).
Dissolucytosis:	Dissolucytosis is the process where macrophages dissolve metal ions from surfaces too large to be phagocytised. Macrophages 'dissolucytes' is believed to form a dissolution membrane, which is chemically controlled by the macrophages, capable of dissolving implant substrates.

Dansk resumé

I Danmark lever ca. 500.000 mennesker med slidgigt og årligt behandles 8000 nye patienter kirurgisk med kunstig hofte. Den umiddelbare bedring af smerter og bevægelighed er særdeles stor, men langtidsholdbarheden kan stadigvæk forbedres. Ti procent af alle hofteproteser løsner sig og vil være udskiftet efter 10 år. Som et svar på dette problem er særdeles holdbare proteser udviklet i CoCrMo legering. Desværre er biokompatibiliteten måske nedsat på grund af cellulære reaktioner på protese legeringen, slidpartikler samt metal ioner frigivet fra legeringen.

Formålet med studierne var at evaluerer biokompatibiliteten af CoCrMo legering, med særlig focus på makrofagers reaktion på legeringen. For det første blev metal frigivelse samt spredning undersøgt i en dyremodel uden mekanisk slid på implantatet. Derudover undersøgte vi makrofagers reaktion på legeringens overflade. I sidste studie undersøgte vi legeringens påvirkning af knogleindvæksten i implantat-knogle zonen.

Vi fandt at metal frigives fra implantater indsat i muskelvæv fra rotter, samt at det akkumuleres i nyre og lever. Desuden fandt vi, at der medfølger en øget metallothionein I/II dannelse i leveren. Vi så at makrofager gav et lavere irritativt respons på legering der var støbt i stedet for smedet, samt lavere end den meget anvendte titanium legering. Knogleindvæksten var dog ikke påvirket af CoCrMo legeringen, der blev dog observeret en dårligere forankring i forhold til den gængse titanium legering.

Studiet giver anledning til overvejelser omkring brugen af CoCrMo. Vi så ingen negativ betydning af CoCrMo legeringen i forhold til knogleindvæksten, men observerede en bekymrende nedsat forankring af CoCrMo implantater. Biokompatibiliteten er ukendt på lang sigt. Kontinuerlig frigivelse af metalioner skal påregnes og teoretisk set er der skabt mulighed for en række bivirkninger.

Abstract

Degenerative joint diseases constitute an increasing problem in public health and are among the most prevalent diseases that affect humans. In Denmark approximately 500.000 people live with the disease, and hip osteoarthrosis alone accounts for 8000 primary joint arthroplasties yearly [1,2]. The present treatment of end-stage degenerative joint disorder relies on replacement surgery using joint arthroplasties. While joint replacement provides compelling pain relief and restoration of function, there is great room for improvement. Despite major advances during the last decades serious problems exist concerning long-term durability and rejection of the artificial joint implants. Ten percent of patients undergoing hip joint replacement will develop periprosthetic bone destruction within 10 years of surgery [3,4]. As an answer to these demands very durable bearings are being developed such as metal-on-metal hip replacements made of CoCrMo alloy. But biocompatibility may be compromised because of macrophage interaction with alloy bulk, particulate wear-debris, and metal ions liberated from the alloys.

Aim of the experimental studies

The aim of the presented experimental studies was to evaluate the biocompatibility of CoCrMo alloy in light of the macrophage mediated (dissolucytosis) metal release [5]. The alloy was studied in three different experimental models. First, an *in vivo* study investigating the release and spreading of metal ions from implants not subjected to any mechanical wear. Secondly, i*n vitro* studies isolating the impact of the alloy on macrophages, and thirdly, an *in vivo* study investigating the influence of the alloy on implant osseointegration.

Hypotheses

We hypothesized that intraperitoneal and intramuscularly implanted CoCrMo wire would release metal ions that would be accumulated in kidney and liver. We further hypothesized that the increased metal ion levels would increase metallothioneine expression in kidney and liver.

We hypothesized that CoCrMo alloy would prove less biocompatible and generate a larger macrophage pro-inflammatory response compared to TiAlV alloys. We further hypothesized, that adding hydroxyapatite would increase biocompatibility and decrease macrophage pro-inflammatory response.

We hypothesized that Titanium PoroCoat® would prove a superior overall performance compared to CoCrMo PoroCoat®.

Results

Animals with intramuscular CoCrMo implants accumulated metal in liver and kidney and metallohionein I/II were elevated in liver tissue. We observed that as-cast high carbon CoCrMo reduced the pro-inflammatory macrophage cytokine response, and that hydroxyapatite coating increased the pro-inflammatory response. Osseointegration was not statistically significant affected by CoCrMo; however, a statistical significant decreased mechanical implant fixation, could be recognized.

Conclusion

In conclusion, these results substantiate considerations regarding the use of CoCrMo. The short-term biocompatibility was affected by a decreased mechanical implant fixation; however, the osseointegration was not affected. The long-term biocompatibility is still to be revealed. A continuous burden of wear particles and metal ions should be encountered, and theoretically many untoward effects may exist.

Background

CoCrMo alloy in orthopedic implant surgery

CoCrMo overview

CoCrMo alloy is used in hip prosthesis manufacturing. It is very durable, biocompatible and has been used since 1930. In the sixties McKee-Farrar metal-on-metal (MOM) [6] implants were introduced, and later in the nineties 300.000 Metasul was implanted [7]. The first implants were used with only limited success; however, some continued to function well into the second and third decade. Careful analyses of these successful cases laid the ground for second-generation MOM hip prostheses made of CoCrMo alloy. Because of elastic modulus close to bone-cement, CoCrMo femur stems has with success also been widely used as cemented stems [8,9]. The alloy consists of 62% - 67% cobalt and 27-30 % chrome, but also include 5-7 % molybdenum and all together under 1 % of manganese, iron, nickel, and silicon [10]. Carbon is added to further improve durability. The alloy is available in either wrought low carbon (LC) (0.07 wt %), wrought high carbon (HC) (0.2-0.35 wt %), or cast CoCrMo [10]. In contrast to the conventional metal on polyethylene hip implants the alloys used in MOM are usually high carbon. Wear properties are better, and linear wear in second-generation MOM is 100 times lower than metal-on-PE in *in vitro* studies [11,12]. This experimental finding has been confirmed in several retrieval studies. The volumetric wear is reduced up to 60 times in MOM compared with metal – on – polyethylene bearings [13,14]. The volumetric wear rate for second-generation MOM is up to one or two orders of magnitude lower than the clinical wear rates for first-generation MOM hip prostheses [12].

Manufacturing commercial CoCrMo implants

Advanced manufacturing techniques have made it possible to create promising MOM prostheses. Using cast manufacturing technologies makes it easier to produce complex prosthetic designs of high quality with very low tolerances as in resurfacing prostheses. The main technological differences between commercial products are, beside casting or forging, carbide content and morphology. Carbide content and morphology can be regulated by carbon content and by heat treating the alloy. Hot isostatic pressing process is used to remove tiny air bubbles along carbide boundaries created during the casting process. Solution annealing changes the large carbide grains in as-cast to fine evenly distributed carbide grains comparable with wrought CoCrMo. No obvious improvements of wear properties have, on the other hand, been reported [10].

Metal debris

Total hip arthroplasties have multiple sources that can release metal debris. Metal wear particles are primarily generated by the articulating surfaces, but also from “fretting corrosion” of screws and head against stem [15]. Nano-sized (25-36 nm) wear particles are generated and constitute of oxide (Cr_2O_3, CoO, Al_2O_3), hydroxide ($CrOH_3$, $CoOH_2$, etc), metal phosphates ($CrPO_4$, $Co_3(PO_4)_2$), or metal (CoCrMo) [12,16-19]. When the stable oxide layer is mechanically disrupted flow of metal ions occur. Metal oxide particles are generated, and metal ions are dissolved from the base of the alloy while the oxide film is restored [20]. Metal ions can theoretically arise from mechanically wear (mainly bearing surfaces), but also from dissolucytosis (Fig. 1) (macrophage dependent corrosion) of wear debris and implant surface (Cr^{3+}, Co^{2+}, Ni^{2+}, Fe^{3+}, Cr^{6+}) [12,16-19]. Implants not subjected to any mechanical stress will still release metal ions [21-23].

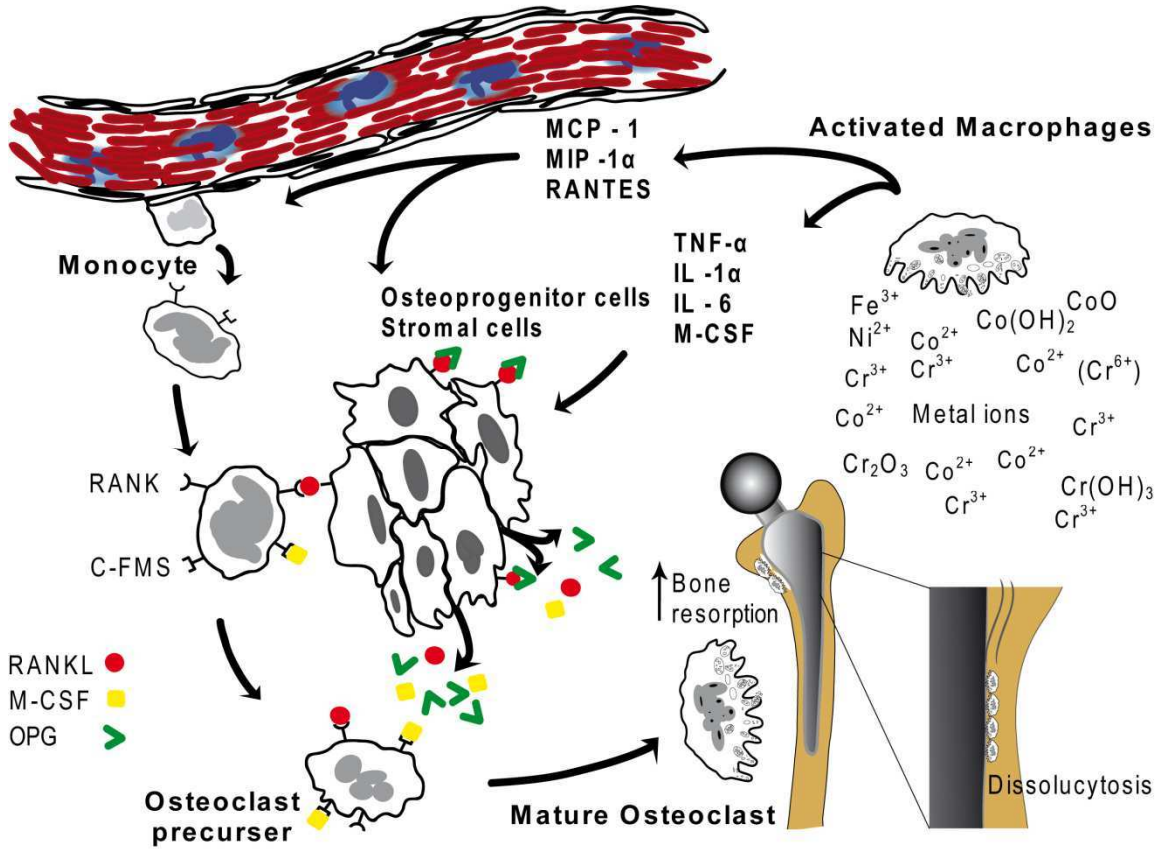

Figure 1. Macrophage pro-inflammatory response increase bone resorption. Macrophages interact with implant surfaces (dissolucytosis), and metal ions and pro-inflammatory cytokines are released. Monocyte attraction, osteoclast differentiation, and osteoclast activation might result in increased bone resorption.

Biocompatibility

"Biocompatibility is the ability of a material to perform with an appropriate host response in a specific application" – WIKIPEDIA

It is not possible to perform a single test that defines whether a certain material is biocompatible or not. The diverse use of materials in different tissue surroundings at altering exposure periods emphasizes the differentiation needed for medical implant materials. Historically, there has been a battle between durability and biocompatibility. For orthopedic implants, long-term durability may compromise short term osseointegration and long term toxicology. Short-term biocompatibility may compromise long-term durability describing the dilemma that we are facing.

Long-term biocompatibility

Potential concerns

Particulate wear debris from orthopedic implants has been found to accumulate in tissue close to the implant, but also in distant lymph nodes, bone marrow, liver, and spleen [24]. And metal ions have been shown to be excreted in the urine [19] and through the bile [25]. Unwanted

side-effects could be seen as a result of the alloy bulk, the released metal ions [19], and wear particles released from the implants [12,16-19]. The number of metal wear particles has been found to be 13 to 500 times higher than the number of wear polyethylene particles released from conventional hip prostheses [16,26]. The large amount of nano-metal particles and metal ions, and the increasing use of metal-on-metal hip prostheses lead to concerns about carcinogenicity [18,27-32], hypersensitivity [33-36], local tissue toxicity [24,37-40], inflammation [41-46], genotoxicity [47,48], and teratogenic effects [48-51].

Short-term biocompatibility

Overview

When an orthopedic prosthetic device is implanted, within a few milliseconds, water, circulating proteins, and other molecules form a biolayer up to approximately 10-100 nm from the surface [52]. Secondly, cells start to migrate towards the prosthesis and adhere to the surface. Macrophages are some of the first cells to arrive at the tissue-implant interface and readily starts to interact with the implant-surface [53,54]. Even though a very inert and stable oxide layer is formed on the implant surface complement system is activated primarily through the alternative pathway [55]. C3 adsorb to the surface as C3b and complexes with complement factor B or factor H resulting in formation of C3b or iC3B respectively. C3b and iC3B are ligands for macrophage surface receptors (CD35, CD11b/CD18, CD11c/CD18) [56]. Fibronectin and vitronectin also adsorb to implant surface, and act as a ligand for macrophages through RGD-integrin receptor domains. These ligand-interactions and several others are the primary interaction between surface and cells [57].

Implant biocompatibility in relation to osseous would healing is mainly determined by cell-implant interactions. The interaction is influenced by chemical composition of the surface [58-61], by surface topography, surface hydrophobicity and possible by other surface factors [62-66].

Macrophage

Macrophages are essential determinants of implant biocompatibility since they are the “first line of defense”. Pro-inflammatory studies show that during the first 6 weeks macrophages interact heavily with the prosthetic device [67,68]. Ideally, both bulk material and any wear product have to be biocompatible, and in the current understanding of aseptic loosening (polyethylene wear particles) macrophages are essential. Macrophages are considered the most important immunological player in aseptic loosening of orthopedic implants [69,70]. Moreover, many of the observed features of macrophages exposed to polyethylene can be found when macrophages meets a “foreign body/implant” larger than the phagocytosable size. Macrophages secrete pro-inflammatory cytokines, and the response generated by particles is, to some extent, independent of the internalization of wear-particles [71]. Cells treated with cytochalasin B (blocks the internalization process) still exhibit a pro-inflammatory response [72,73].

Macrophages react with ultra high molecular weight polyethylene (UHMWPE) wear particles by expressing and/or releasing pro-inflammatory, proliferate, and chemoattractant cytokines (IL-1α, IL-1β, IL-6, TNF-α, MIP-1α, RANTES, M-CSF, MCP-1). These cytokines and numerous degrading molecules (collagenases, gelatinases, stromolysin, extracellular matrix metalloproteinase inducer, cathepsin C, α-1 antihymotrypsin, tenascin, elastase) are found in the proximity of loose implants [69,74-77].

The result is monocyte attraction, transformation of the immature macrophages to osteoclasts, prolonged survival of the osteoclast, resulting in an increased bone resorption.

Macrophages also play an important role in wound repair and bone remodeling by acting as a reservoir for bone-regulating cytokines. BMP-2, a member of the TGF-β superfamily have a well characterized function in bone induction [78,79]. TGF-β is also important in osseous wound healing [80,81] through stimulation of collagen synthesis combined with an inhibition of collagen degradation by fibroblasts [82]. OPG is a decoy protein that blocks the RANK-RANKL ligation by competitive binding to RANKL sites on stromal cells [83]. The release of IL-10 is stimulated by pro-inflammatory cytokines TNF-α, IL-1, and PGE2, and has a down regulating effect on pro-inflammatory cytokines (IL-1α and β, TNF-α, M-CSF, IL-6) and reactive oxygen species (O_2^-, NO). IL-10 also down regulates MHC-II hence antigen presenting function. Finally, it stimulates apoptosis in human monocytes by up-regulating the CD95 receptor [70].

Osteoclasts

Osteoclasts are the final common pathway in osteolysis and are dependent on number, activity level, and survival rate. Osteoclast resorption is greatly regulated by cytokines.
Monocytes and macrophages (osteoclast precursors) are attracted by the C-C chemokine group, a subfamily of chemokines; MCP-1-4, MIP-1α, 1β, 3α, 3β, and RANTES, increases. MCP-1 attracts monocytes, macrophages, and plays a key role in immunoregulatory and pro-inflammatory processes regarding wound healing [84]. Osteoclast number increases when monocytes differentiate into osteoclasts. With or without RANKL present, monocytes exposed to M-CSF (through the c-fms receptor) differentiates into osteoclasts [75,85]. Retrieved osteolytic periprosthetic tissues demonstrates high MCP-1 and MIP-1α expression [75]. Osteoclast survival rate is increased by TNF-α [86], and TNF-α generates both directly [85], and especially with permissive levels of RANKL, osteolysis by transforming osteoclast precursors to mature osteoclasts [87]. Extremely low levels of TNF-α (100 pg/ml) is sufficient to activate resident un-activated osteoclasts [88]. In general TNF-α is a key mediator of the inflammatory process, and contributes greatly also to the reparatory phase either directly influencing endothelial and fibroblast functions or indirectly by inducing additional cytokines and growth factors [89]. TNF-α stimulates osteoclastic activity and regulates osteoblast proliferation [90,91]. IL-6 induces epithelisation, and influences granulation tissue formation during normal wound healing. IL-6 also induces osteoclast formation and consequently is involved in both bone resorption and bone formation in the remodeling stage [92,93]. IL-6 is found in abundance in tissue surrounding failed hip-prosthesis [75].

Osteoblasts

The remodeling of the bone is a continuously process, throughout the entire human life, with osteoclast resorption and osteoblast formation representing a delicate state of equilibrium. Implants present a continuous source of wear particles and metal ions through-out the entire implant life potentially able to locally affect this state of equilibrium [94] (Fig. 2). The equilibrium is also affected by age. From a positive bone turnover in the adolescent most people will experience a negative bone turnover from the age of 50. Osteoblasts are derived from mesenchymal stem cells, and are continuously replaced since they get entrapped in the mineralized bone as osteocytes and/or undergo apoptosis.
Boneformation is regulated both systemically (parathyroid hormone, calcitriol, growth hormone, glucocorticoids, thyroid hormones, sex hormones) and locally [95]. Local bone forming factors are insulin-like growth factors (IGFs), prostaglandins, tumor growth factor-β (TGF-β), bone morphogenetic proteins (BMP). Osteoblasts also regulate the boneresorption, and potentially act both positively and negatively on bone turnover. Osteoblasts express RANKL and M-CSF and are thereby osteolytic [96,97], but osteoblast also express OPG and are thereby also bone conserving [98].

Osseointegration in relation to metal ions

Bone healing in relation to implantation can be considered as a series of events, where the final result and success is dependent on each of these events. In osseous wound healing several cell-types including osteoblasts, osteoclast, and macrophages all play a pivotal role with the ability to affect the above mentioned series of events in a deleterious way, essentially making an implant fail (inferior results) (Fig. 2). Dissoluted metal ions from the implant surface are known to affect peri-implant cells in particular osteoblast [22,23]. MG-3 osteoblast, fibroblasts, and lymphocytes proliferation are susceptible to metal ions in particular Vanadium, Nickel, and Cobalt [99]. Apoptosis and/or necrosis are induced in a wide range of cells by metal ions liberated from implant material [100]. Released Co and V are more cytotoxic [18], than Al, Fe, Cr, and Mo; however, these ions seems to suppress osteoblast proliferation more than fibroblasts proliferation [99]. Previously, research has suggested that a threshold level must be reached (Co – 0.8 mM for both fibroblasts and osteoblasts; V – 0.1 mM respectively 0.4 mM) to negatively influence cells [99]. CoCrMo implant surface itself and metal debris may also be involved in the complex cellular and molecular response in osseous wound healing by inducing cytokine response [42,101] that affects proliferation and necrosis/apoptosis [99,102].

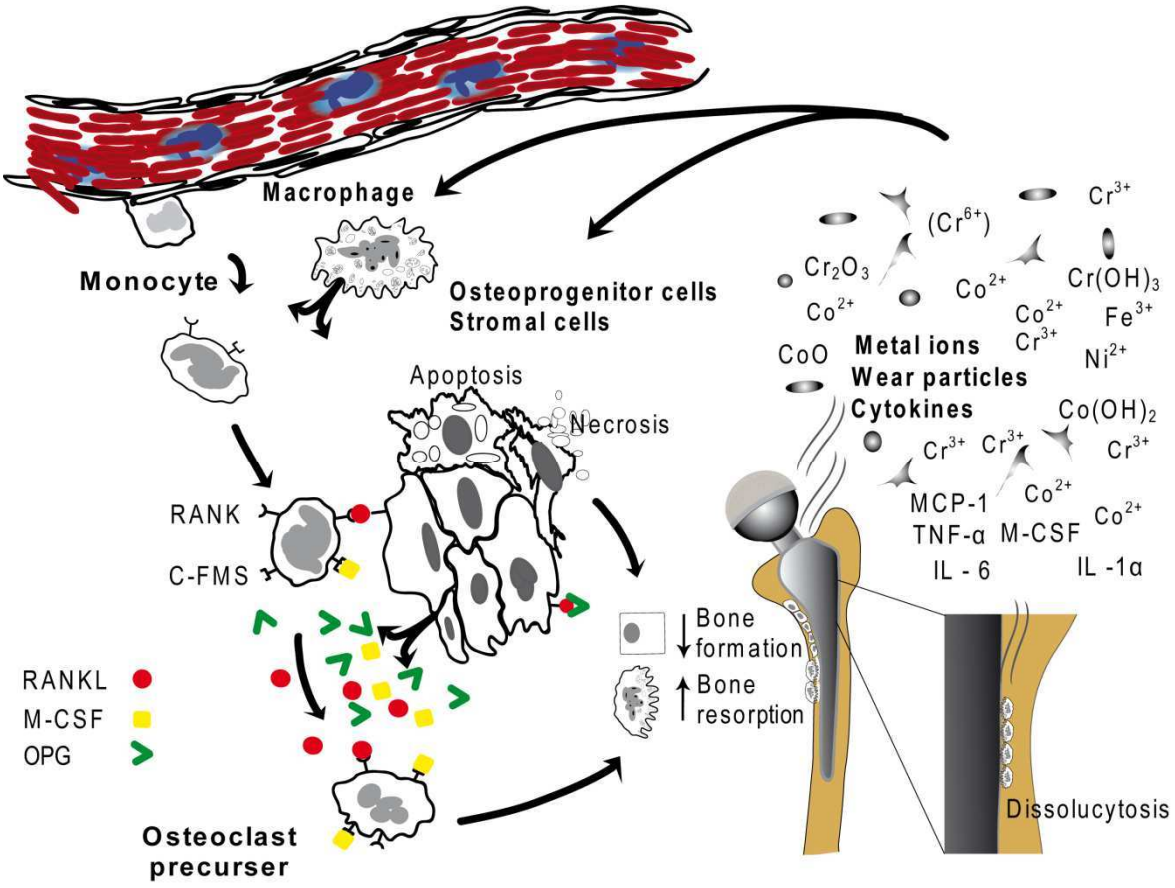

Figure 2. Proposed negative influence on the state of equilibrium bone turnover by metal ions and wear particles in relation to orthopedic implant. Macrophages interact with implant surface by dissolucytosis, and metal ions and pro-inflammatory cytokines are released. Mechanical wear on bearing surfaces generates particulate and ionic wear. Exposed macrophages generate a pro-inflammatory response capable of increasing bone-resorption. Exposed osteoprogenitor cells, osteoblasts, and stromal cells may undergo apoptosis, necrosis, or may have decreased proliferation and function essentially resulting in decreased bone formation.

Materials and Methods

Metal release from CoCrMo implants - Accumulation in kidney and liver (Study I)

Design of study

The study was a three-armed animal study where intraperitoneally-, intramuscularly-, and non-exposed animals were compared in respect to metal ion concentration (PIXE) and metallothionein I/II levels (real time RT-PCR) in liver and kidney tissue. Group one had a CoCrMo wire (Ø = 0.1001 mm; L = 20 cm coiled ASTM F-75 CoCrMo) implanted in their gastrocnemic muscle of the left leg. Group two had the wire implanted intraperitoneally, and group three was sham-operated (Fig. 3). Sample size was considered as following: error of the first kind (2α) was selected to 5%. Based on previous studies a standard deviation of 10% on PIXE analyses of relevant atoms were used [103]. MIREDIF was set to be 70%. Error of the second kind (β), the risk of false negative result, was set to be 20% which means a power of 80%. Based on these assumptions, using G*Power software, tissue samples from at least 9 experimental animals had to be included [104].

Methodological Considerations

Rats together with mice are preferred animals when conducting toxicological studies because of ethical considerations with larger animals. Caution when extrapolating the results should; however, be attained. Detoxifying/pacifying routes, pharmacokinetics, and toxicological effects are not necessary the same as in humans.

The observation period for this study was 9 month. We wanted the animals to be able to achieve a steady state condition, where we would expect the exposure of metal ions, the detoxifying routes, and excretions organs to be in steady state. We did pilot studies on rats at both 3 and 6 month, where multiple kidney and liver tissue sections was examined histological (autometallografic developed, constant stain with touluidin blue) and with PIXE analyses to asses metal concentration and impact on the tissue. We did not observe any statistically significant difference metal ion concentration at these time points (Data not presented). We did not either observe any histopathological changes of the tissue.

To avoid any biased contamination the animals were all obtained from the same supplier at the same time for the study. The animals were kept in plastic cages in the same room, and were fed a special metal controlled diet. The sham group was also anesthetized, and a syringe was placed in the abdominal cavity respectively gastrocnemic muscle mimicking the procedure used to place the coiled up metal threads in the exposed animals.

After 9-month exposure, the animals were anesthetized and sacrificed by decapitation and processed randomly. The coiled CoCrMo wire located/embedded in the surrounding connective tissue were identified intra-abdominally and intramuscularly in all exposed rats.

Animals

Twenty-seven 3-months-old male Wistar rats were used for the study. The animals were kept in plastic cages in a room with a 12-hr light/dark cycle at 21-22^{o}C and 50 % humidity. They were fed with Altromin No. 1324 (Spezialfutterwerke, Germany) ad libitum and had free access to tap water. The study was undertaken in accordance with the Danish and University of Aarhus guidelines for animal welfare.

Exposure

A 0.1001-mm thick coiled ASTM F-75 CoCrMo wire was kindly donated by Fort Wayne Metals, Research Products Corp. Indiana, USA. This alloy consists of 27.45 % Chromium, 5.70 % Molybdenum, 0.66 % Manganese, 0.64 % Silicon, 0.27 % Iron, 0.142 % Nitrogen, 0.09 % Nickel, 0.01 % Carbon, and balanced with 65.038 % Cobalt.

The CoCrMo wires were cut in 20-cm pieces, coiled, and placed in a BD Microlance^{TM} 3 18G, 1½" syringe (BD A/S, Denmark). The average weight of each piece of wire was 0.0143-g (SD = 0.0002708g). The animals were anesthetized with Isofluran Baxter (Baxter A/S, Denmark), and the coiled metal was injected in the rat. A stylus was used to press the coiled metal out of the needle leaving it intraperitoneally or intramuscularly for a 9-month exposure time. The sham group was anesthetized, and a syringe was placed in the abdominal cavity respectively gastrocnemic muscle mimicking the procedure used to place the coiled up metal threads in the experimental animals. The animals was obtained from the same supplier at the same time, were feed the same, kept in the same cages, and kept in the same room in the stable as the exposed groups.

After 9-month exposure, the animals were anesthetized with Isofluran inhalation and Mebumal intraperitoneal injection. The deeply anesthetized animals were sacrificed by decapitation and processed randomly. First, kidney and liver were removed, sectioned and a part was snap frozen in liquid nitrogen, and finally, a part was frozen with CO_2. The coiled CoCrMo wire and the connective tissue surrounding were identified intra-abdominally and intramuscularly in all exposed rats.

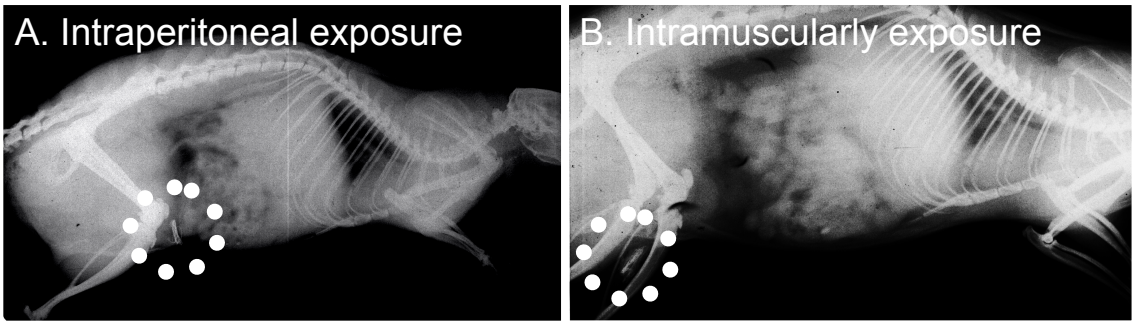

Figure 3. X-ray pictures of exposed animals. Intramuscularly exposed animals (B) accumulated more metal in their kidney and livers compared to intraabdominal exposed animals (A) and expressed higher levels of methallothionein I/II in their livers.

PIXE analyses

In PIXE (proton induced x-ray emission) neutrons are bombarded on the non-treated 60-µm thick cryosections of kidney and liver tissue [105,106]. Neutrons knock out electrons leaving empty states around atoms. X-rays specific for the affected atoms are emitted when the empty states are filled again with electrons from outer states. The PIXE analysis gives information about the absolute amounts of the elements present within the beam spot. However, because of the irregular shape of the sections and also to some variations in their thicknesses, the results could not be converted directly to concentrations in the tissue. Therefore it was necessary to normalize the data using one of the most abundant elements, and assuming that it was present in the same concentration in all of the analyzed types of tissue. As the actual mass of tissue exposed to the proton beam is not known, the metal content was normalized towards a standard of (Potassium) K = 17.300 µg/g [105]. The detection limit is approx 10^{-13} g of the matter of interest (0.1 ppm) in the entire sample, that is the total amount of the mater (dry weight) in the sample, independently of how it its present. The detection limit is not as low as ICP-MS; however, the sample does not have to be "opened" which makes the method

more resistant to contamination. The 60-µm thick kidney and liver sections were treated and analyzed as previously described [107].

Real time RT-PCR

Immediately after retrieval of tissue it was snap frozen in liquid nitrogen and stored at – 80^{o}C until RNA extraction. 2 x 2 x 2 mm pieces of tissue were homogenized thoroughly using a RETSCH (RETSCH GmbH, Germany) bead homogenizer with 1 ml TRIZOL® Reagent (Invitrogen™, life technologies, Denmark), and samples were treated as described previously [107].

To minimize the effect of variations in the housekeeping enzymes, we normalized to a BestKeeper index [108] calculated for each sample based on a geometric mean of threshold cycles (Ct) from GAPDH and UBC. The following equation was used for each biological sample: relative gene of interest expression = $2^{Ct\ (best\ Keeper)-Ct\ (gene\ of\ interest)}$.

CoCrMo and TiAlV – (Study II)

Design of study

This was an experimental five-armed *in vitro* cell-study where J774A.1 mouse macrophages (ATCC, Rockville, MD, USA) were exposed to different implant materials, and the cytokine response (TNF-α, IL-6, IL-1α, IL-1β, IL-10, M-CSF, MCP-1, TGF-β, OPG) were evaluated on protein level (ELISA) and on transcription level (real time RT-PCR) (Table 1).

Methodological Considerations

J774A.1 was incubated 8-hours with either as-cast HC CoCrMo, wrought HC CoCrMo, wrought LC CoCrMo, or wrought TiAlV (kindly donated by Biomet Inc., Warsaw, IN, USA). Experiments were conducted after 4-8 passages. Negative controls were done without the discs.

We used the mouse cell line J774.A1 because of the close resemblance to macrophages seen in the proximity of implants and cement in humans [109-111]. Non-stimulated J774A.1 tends to be less activated than isolated human monocytes/macrophages and thereby creating a more uniform pro-inflammatory response. The J774A.1 cell line have demonstrated several effects (patterns) comparable to that of human macrophages, *e.g.,* phagocytosis, transcription, and release of pro-inflammatory cytokines when activated; transcription and release of TGF-β, transcription of BMP-2 at rest (non-activated); and finally the ability to spread out on a surface [109-112]. In agreement with these reports, we have in the present study and other ongoing studies observed the same basic features in our J774A.1 cell line – *e.g.* the ability to perform phagocytosis of specific particles (CoCrMo, Gold, Platinum, polyethylene), to release and/or transcript a wide variety of cytokines (*e.g.,* TNF-α, IL-1α, IL-1β, IL-4, IL-6, MCP-1, M-CSF, OPG, TGF-β, IL-10) in response to various stimuli (*e.g.* CoCrMo discs, Titanium discs, and Ultra High Molecular Polyethylene discs as well as commercial 3D-surfaces, and Lipopolysacharide), and to out spread on a surface (gold).

LPS time-course and dose-response studies were performed to follow the course of both mRNA and protein production (Fig. 5). The results indicate that, for TNF-α, IL-6, and MCP-1 8-hours incubation was ideal. Ideally time-course experiments should be done with metal discs; however, the response generated is so small that this would be very impractical. Time-course experiments indicate that optimum incubation time for mRNA assays would be 4-6 hours, but time-course experiments were done on LPS activated macrophages which undoubtedly generates an earlier response compared to metal-surfaces. The protein secretion for the examined cytokines peaks 2-3 hours later than the mRNA expression, leaving 8 hours incubation time optimal for both protein secretion and mRNA transcription.

We investigated cytokines important for bone resorption that have been observed in tissue from clinical cases of aseptic loosening (pro-inflammatory, chemotaxis, and proliferation) [75,76], and we also investigated an anti-inflammatory and bone generating response. All cytokines were known to be secreted by human macrophages. Studies performed in cell lines/cultures often provide early pieces of information only, which has to be further investigated in more advanced models to be able to extrapolate into a human context. Cell lines; nevertheless, still provides valuable information when trying to control the number of variables in biomedical research.

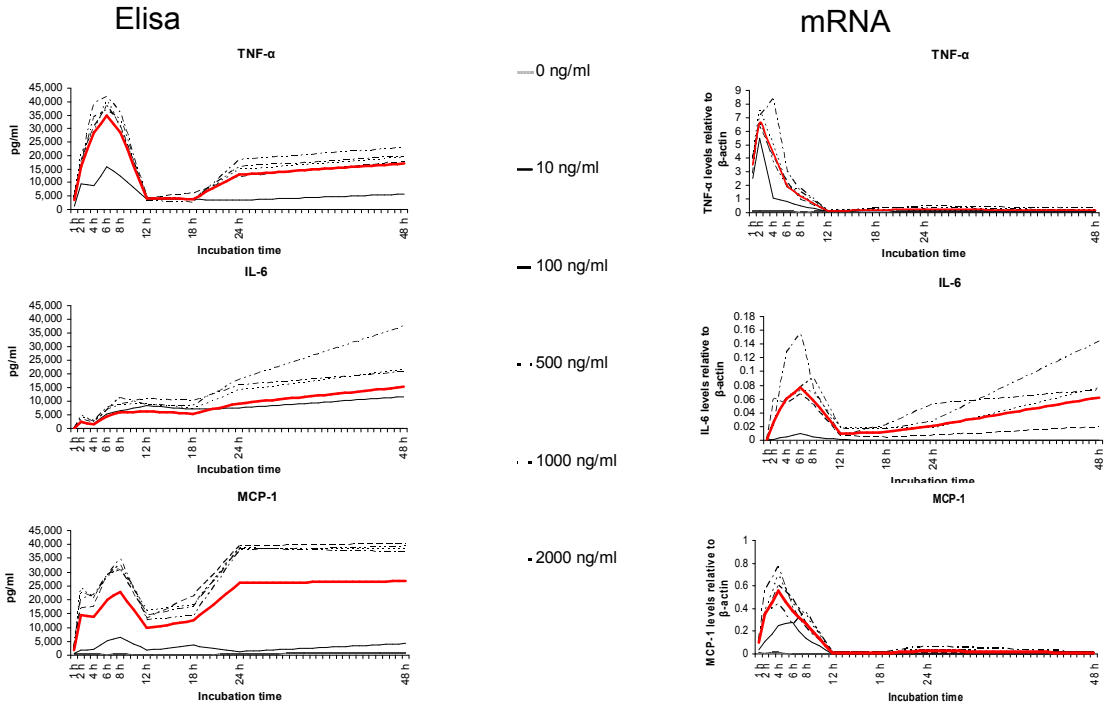

Figure 5. **Time-Course and Dose Response.** TNF-α, IL-6 and MCP-1 protein release and mRNA transcription from time-course and dose response studies. Mean result is represented by a red line. LPS was used as activator.

Plasmaspray- and porouscoating ± HA (Study III)

Design of study

This was an experimental five-armed *in vitro* cell-study where J774A.1 mouse macrophages (ATCC, Rockville, MD, USA) ± LPS pre-exposure were exposed to different surface coatings, and the cytokine response (TNF-α, IL-6, BMP-2, and TGF-β) were evaluated on protein level (ELISA), and on transcription level (real time RT-PCR) (Table 1).

Methodological Considerations

This study was based on the model as previously described [113]; however, some adjustments were made. First, LPS activated and non-activated J774A.1 mouse macrophage was incubated 24 hours with plasmaspray ± HA (kindly donated by Biomet Inc., Warsaw, IN, USA). Secondly, non-activated J774A.1 cells were incubated either 6 or 24 hours with plasmaspray ± HA or porouscoating ± HA (Smith & Nephew Orthopedics, Inc., Memphis, TN, USA). The bone inductive cytokine response (TGF-β, BMP-2) was examined after 24 hours leaving the

macrophages time to interact with the surfaces [112,114,115] without the need for adding additional medium.
Both HA and titanium coating procedures and packaging procedures are under continuously endotoxin control. Surface element composition was evaluated with EDS, which showed presence of Titanium, Aluminium, and Vanadium on the discs without HA, and in addition large amounts of Oxygen, Phosphate, and Calcium on HA coated discs.

Table 1. Study II and III

Material type	Substrate Material	Ave. Roughness**	Number (N) / time (h)	Macrophage pre-activation (LPS)	Endotoxin	Cytokines
Study II		Rough / Polished				
Wrought CoCrMo HC	CoCrMo	718 nm/6.3 nm	5*/8h	No	0.14 EU/ml	IL-1α, IL-1β, IL-6, IL-10, TGF- β, TNF- α, M-CSF, MCP-1, OPG
Wrought CoCrMo LC	CoCrMo	546 nm/7.0 nm	5*/8h	No	0.14 EU/ml	IL-1α, IL-1β, IL-6, IL-10, TGF- β, TNF- α, M-CSF, MCP-1, OPG
As-Cast CoCrMo HC	CoCrMo	351 nm/12.5 nm	5*/8h	No	0.14 EU/ml	IL-1α, IL-1β, IL-6, IL-10, TGF- β, TNF- α, M-CSF, MCP-1, OPG
Wrought Ti6Al4V	Ti6Al4V	340 nm/21 nm	5*/8h	No	0.14 EU/ml	IL-1α, IL-1β, IL-6, IL-10, TGF- β, TNF- α, M-CSF, MCP-1, OPG
Study III		+HA / -HA				
Plasmaspray Coating Ti6Al4V ± Hydroxyapatite	Ti6Al4V	40.1 µm/34.1 µm	10/6h-24h	Yes	N/A ***	TNF- α, IL-6, TGF- β, BMP-2
Porous Coating Ti6Al4V ± Hydroxyapatite	Ti6Al4V	31.8 µm/19.0 µm	10/6h-24	No	N/A ***	TNF- α, IL-6,

HC – High Carbon, LC – Low Carbon, (0.14 EU/ml ± 0.04 SEM)
* Experiments were done twice and data were pooled.
** In study III roughness were evaluated with profilometer, and in study IV roughness were evaluated with confocal laser scanning microscope.
*** No contamination. The production line is under continuously endotoxin control.

Technical methods (Study II and III)

Cell culture

J774A.1 mouse macrophages (ATCC, Rockville, MD, USA) were exposed to implant material discs. Cells were maintained under standard culture conditions as described [113,116]. In study II, 5-ml medium containing 5.0 x 10^6 cells were placed on the discs in Nucleon™ Δ Surface 6 wells dishes (Nunc). After 8 hours supernatant were separated from the cells and frozen at -20°C. Cells were harvested with a plastic cell scraper, centrifuged, and quenched in liquid nitrogen and stored at -80°C until further analyses. Discs were studied with n=5, and experiments were done two times and the data were pooled.
In study III, 2 ml medium containing 2.0 x 10^6 cells were placed on the discs in Nucleon™ Δ Surface 24 wells dishes (Nunc, Roskilde, Denmark). After 6 and 24 hours the adherent cells were harvested using a cell scraper (Nunc, Roskilde Denmark). Supernatant were separated from the cells and frozen at -20°C and cells were quenched in liquid nitrogen. Discs were studied with n = 10. When investigating BMP-2 and TGF-β production, Lipopolysaccharide (LPS)

(SIGMA, Product no. L8274) - activated and non-activated cells were exposed to Plasmaspray coating ± HA. In the LPS – activated group LPS concentration was 100 ng/ml in the medium.

Table 2. Mouse – Cytokine primers

PCR primers	Sequence	Size
IL-1α	forward, 5'- TTACAGTGAAAACGAAGA -3' reverse, 5'- TGTTTGTCCACATCCTG -3'	418 bp
IL-1β	forward, 5'- CTTCATCTTTGAAGAAGAGCCC -3' reverse, 5'- CTCTGCAGACTCAAACTCCAC -3'	418 bp
IL-6	forward, 5´ TTCACAAGTCCGGACAGGAG 3´ reverse, 5´ TGGTCTTGGTCCTTAGCCAC 3´	488 bp
IL-10	forward, 5' – GGTTGCCAAGCCTTATCGGA -3' reverse, 5'- ACCTGCTCCACTGCCTTGCT -3'	191 bp
TGF-β	forward, 5'- TGGACCGCAACAACGCCATCTATGAGAAAACC-3' reverse, 5'- TGGAGCTGAAGCAATAGTTGGTATCCAGGGCT-3'	525 bp
TNF-α	forward, 5'-CATCTTCTCAAAATTCGAGTGACAA-3' reverse, 5'-TGGGAGTAGACAAGGTACAACCC-3'	175 bp
M-CSF	forward, 5'- TCTCATCAGTTCTATGGCCC -3' reverse, 5'- GGGAGTAGACAAGGTACAAC -3'	212 bp
MCP-1	forward, 5'-CTCACCTGCTGCTACTCATTC-3' reverse, 5'-GCTTGAGGTGGTTGTGGAAAA-3'	317 bp
OPG	forward, 5'-TCCTGGCACCTACCTAAAACAGCA-3' reverse, 5'-CTACACTCTCGGCATTCACTTTGG-3'	578 bp
BMP-2	forward, 5'- GACGGACTGCGGTCTCCTAAAG -3' reverse, 5'- TCTGCAGATGTGAGAAACTCGTCA -3'	479 bp
ß-actin	forward, 5'-CCCACTCCTAAGAGGAGGATG-3' reverse, 5'-AGGGAGACCAAAGCCTTCAT-3'	214bp

Protocol: Intro: 95°C in 15 minutes. Denature: 95°C in 30 seconds. Anneal: 57°C in 30 seconds. Extension: 74°C in 60 seconds.
Fluorescence is measured in the Extension-phase.

Protein levels of cytokines

Supernatant from the cultures was, as previously described [113], thawed and analyzed for the cytokines using a commercially available ELISA kit. TGF-β and BMP-2 are both present in cell media, therefore we established the cytokine levels in the media before adding cells and subtracted that from the final result after the exposure.

When analyzing IL-6 levels in study III (HA) the protein levels were very low, why we extended the standard curve by two points enabling us to quantify the low IL-6 levels. The data variation increases compared to the variations of data within the normal standard curve. We observed a large variation; however we did anyway observe at statistically significant increase.

When encountering non-detectable low results (OPG, BMP-2), we spiked the supernatant with the cytokines to verify the efficiency of the assays.

Real time RT-PCR

Real time RT-PCR was performed as described by Jakobsen *et al*. [113]. Briefly, TRIZOL® Reagent (InvitrogenTM, life technologies, Taastrup, Denmark) was used to extract the mRNA then three steps follow. First homogenization, second phase separation, and third RNA precipitation. Measuring the optical density at 260 nm and 280 nm checks quantification of RNA and the ratio should be 1.8 or higher (Gene Quant II, Pharma Biotech, Buckinghamshire, UK). Electrophoresis was done with RNA on a 0.7 % agarose gel. Staining the gel with ethidium bromide makes it possible to see discrete bands which should be between 7 kB and 15 kB in a good quality RNA separation. Each biological sample was run technical doublets for each gene. The primers used are listed in Table 2. Threshold cycles (C_T) were defined as the fractional cycle number at which the fluorescence reached 10 times the standard deviation of the baseline. Relative gene expression of β-actin to cytokines was calculated as $1/(2^{(CT\ Target/CT\ \beta\text{-actin})})$, essentially as described in the manufacturer manual (Perkin Elmer Cetus). β-actin was assumed to be a constant during the experiments.

Assessment of Cell Viability

Cell toxicity was examined in study II by measuring LDH. A possible explanation of the decreased cytokine level for as-cast HC CoCrMo could be cyto-toxicity. If the cells suffer they would maybe not be able to produce cytokines. In necrotic cells the membrane is disrupted and LDH escapes the cell [117]. LDH was measured using a spectrophotometric evaluation of LDH mediated conversion of pyruvic acid to lactic acid (Department of Clinical Biochemistry, Aarhus University Hospital, Denmark). The LDH content did not vary between the cells incubated 8 hours in the empty polystyrene wells compared to cells incubated with discs (empty wells vs. discs, p=0.64, data not shown).

Surface characterization

The specific relationship between surface topography, inflammation, and tissue regeneration has not yet been established, but it has been suggested that roughened surface influence macrophage adhesion, proliferation, and activation [70]. Surface topography in study II (CoCrMo) was characterized with at traditional profilometer Dektak 3030 (Veeco/Sloan Technology Division, Santa Barbara, CA, USA) with a 12.5 µm diamond stylus. Plane and smooth surfaces are fast and very reliable characterized topographically by a profilometer.
Valley-peak heights larger than 200-400 µm exceeds the range of motion for the "pick-up" leaving these 3D-surfaces unsuitable for the traditional profilometer, therefore surface topography in study III was done with Confocal Laser Scanning Microscope (CLSM) (LSM 510 META, Zeiss, Germany fitted with an EPIPLAN Neufluar x 20, 0.5 objective) [118,119].
Commonly used topography parameters from CLSM are larger than corresponding parameters from traditional mechanical stylus instrument (Profilometer). This can be explained by that the mechanical stylus have at tip radius larger than 12.5 µm compared to that of the laser beam which is ≈ 0.5 µm with the possibility to detect deeper valleys than the mechanical stylus [118,119].

Discs

In study II discs were kindly provided by Biomet© USA. Four different types of discs were tested; wrought HC CoCrMo; wrought LC, CoCrMo; as-cast HC CoCrMo; and wrought TiAlV. Three-mm-thick discs were machined out of 15-mm cylinders of the materials. Discs were

polished as described by Jakobsen *et al.* [113]. The surface element composition was verified with EDS (Energy Dispersive System) from EDAX (Mahwah, NJ, USA).
In study III, Porous coated discs ±HA were kindly provided by Smith & Nephew Orthopedics (Inc., Memphis, TN, USA) and Plasmaspray coated discs were kindly provided by Biomet Inc. (Warsaw, IN, USA) (Fig. 6). Discs were 3 mm thick and 15 mm in diameter. Surface element composition was evaluated with EDS, which showed presence of Titanium, Aluminum, and Vanadium on the discs without HA and in addition large amounts of Oxygen, Phosphate, and Calcium on HA coated discs. HA specifications were provided by the manufacturer and the data are presented in Table 3.

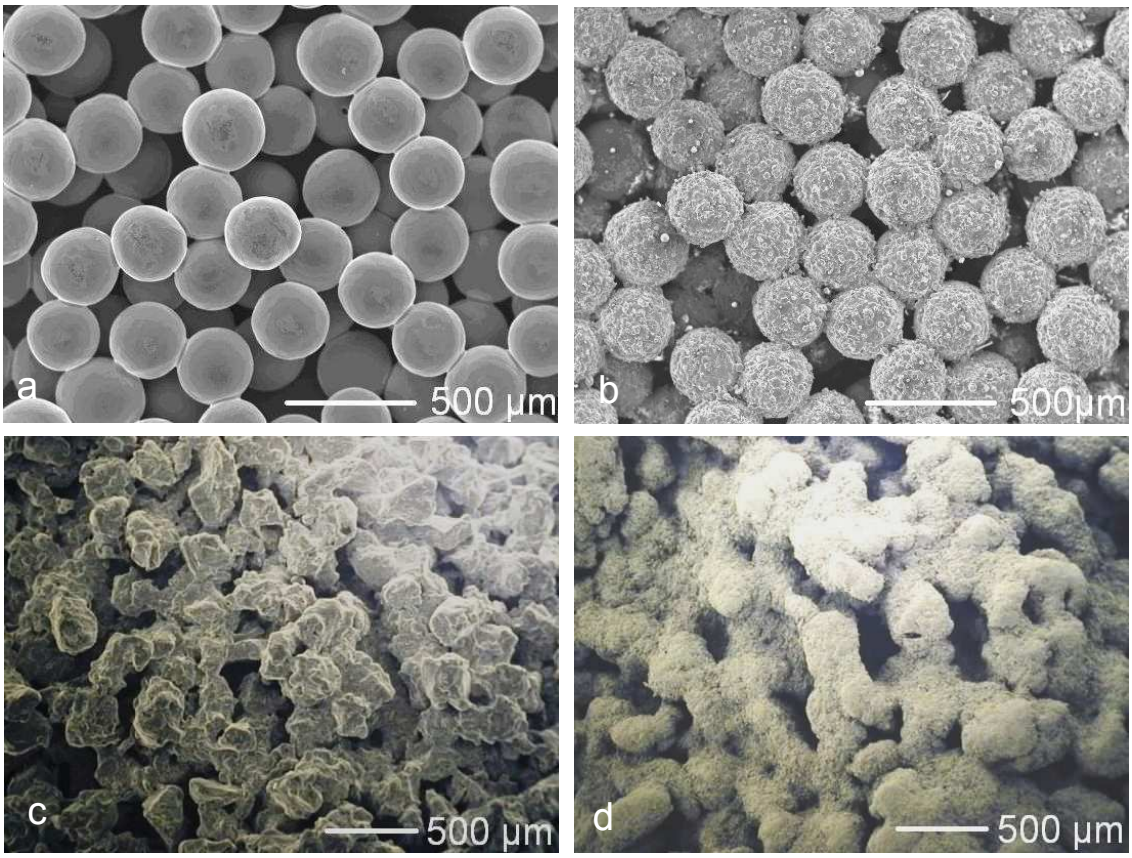

Figure 6: **Scanning electron microscope (SEM) micrographs of the four 3D – surfaces.** a) Titanium porous coated - hydroxyapatite (HA); b) Titanium porous coated + HA; c) Titanium plasmaspray coated - HA; d) Titanium plasmaspray coated + HA. Courtesy of Smith & Nephew Orthopedics, Inc., Memphis, TN, USA and Biomet Inc., Warsaw, IN, USA.

Endotoxin

Endotoxin stimulated macrophages expresses and releases pro-inflammatory cytokines [71]. To be able to isolate the effect of the alloy alone, endotoxin has to be cleared entirely; however, this is not the clinical setting where endotoxin is ubiquitously present. To be able to predict the performance of implant materials, endotoxin has to be taken into account. Certain materials are more prone to be affected by endotoxin as polyethylene where endotoxin is accumulated and is extremely difficult to remove [120-122]. To achieve a physiological endotoxin level in study II [123] discs were cleansed in a single cycle as previously described [120]. Endotoxin testing was done by Cambrex testing services (Cambrex Europe, Verviers, Belgium). In study III discs were delivered gamma-irradiated and treated as the commercial hip products without endotoxin. Both HA and titanium coating procedures and packaging procedures are under continuously endotoxin control.

Table 2. Hydroxyapatite specifications.

Coating type	Tricalcium phosphate (β-TCP)	Purity of HA	Cystalinity of HA	Ca/P-ratio	Thickness of coating
HA on plasmaspray coated titanium	5 wt%	95wt%	62 wt%	1.67	56 - 86 µm
HA on porous coated titanium	3.25 wt%	96.75wt%	77 wt%	1.67	40 – 80 µm

Hydroxyapatite (HA) specifications supplied by the manufacturer. The commercial available HA coatings are applied by plasmaspray technology.

CoCrMo impact on osseointegration (Study IV)

Design of study

The study was designed as an animal study with 10 skeletally mature Labrador dogs (Fig. 7). Mean body weight was 32.3 kg [25 kg: 39 kg]. Each dog had the implants inserted with a 750-µm empty gap in each proximal humerus. Approval was obtained from our Institutional Animal Care and Use Committee prior to performing the study. Sample size was considered as following:

$n1 = n2 = 2(Z_{2\alpha} + Z_{\beta})^2 \times s^2 / MIREDIF^2 = n1 = 2(1.96 + 0.84)^2 \times 50^2/70^2 \sim 8$

Error of the first kind (2α) was selected to 5%. Based on previous studies a SD of 50 was used and MIREDIF was set to be 70. Error of the second kind (β), the risk of false negative result, was set to be 20% which means a power of 80%. Based on these assumptions at least 8 experimental animals had to be included. Therefore we included 10 animals in each group to allow loss of 2 individual.

Methodological Considerations

Our experimental 750-µm gap model was designed to imitate the close interaction between cementless joint replacement alloys and bone forming/remodeling process in cancellous bone. We used a clinically well-proven implant coating for un-cemented implants, PoroCoat®, where the only difference between the coatings was the metal composition. Canine cancellous epiphyseal bone was chosen because the close resemblance with bone where cementless joint replacements are usually implanted. Canine bone reflects the composition, density, and quality of human bone better than that of most other animals [124]. No animal model, however, gives complete information about the effect of a given alloy on human osteogenesis. Canine bone remodels three times faster than humans, and all implants were put in healthy bone of young dogs. The model lacks clinically relevant influences such as joint fluid pressure, direct load, revision environment, and cement. This is a basic experimental model that is more controlled than other weight bearings models [125].

A statistically significant difference in all parameters between upper and lower hole existed and could be manage well by using 2-way ANOVA statistical test. But two-way ANOVA is only valid on parametric data with equal variance. Variation of non-parametric data could not be managed this way and hence the IQR were larger, increasing the risk of overlooking an existing difference.

Surgical procedure

Under general anesthesia, using sterile technique, the proximal part of humerus was exposed through a lateral extraarticular approach. Two Kirschner (K) wires were inserted perpendicular to the surface with 17.0-mm in-between. The most proximal K wire was inserted at the level of the greater tubercle. The K wires were used to guide a 7.5-mm canulated drill when making a 13.0-mm-deep hole. Drilling was performed at 2 rotations per second to prevent thermal trauma to the bone. All bone debris and soft tissue was removed from the drill hole and the implant with the footplate was inserted, leaving the gap between implants and bone tissue empty. Finally, the top washer was mounted and soft tissue closed in layers. Pre- and postoperatively, the dogs were given one dose of cefuroxim, 1.5 g intravenously, as antibiotic prophylaxis. A fentanyl transdermal patch (75 µg/h) lasting 3 days was given as postoperative analgesic treatment. The dogs were allowed full weight bearing postoperatively.

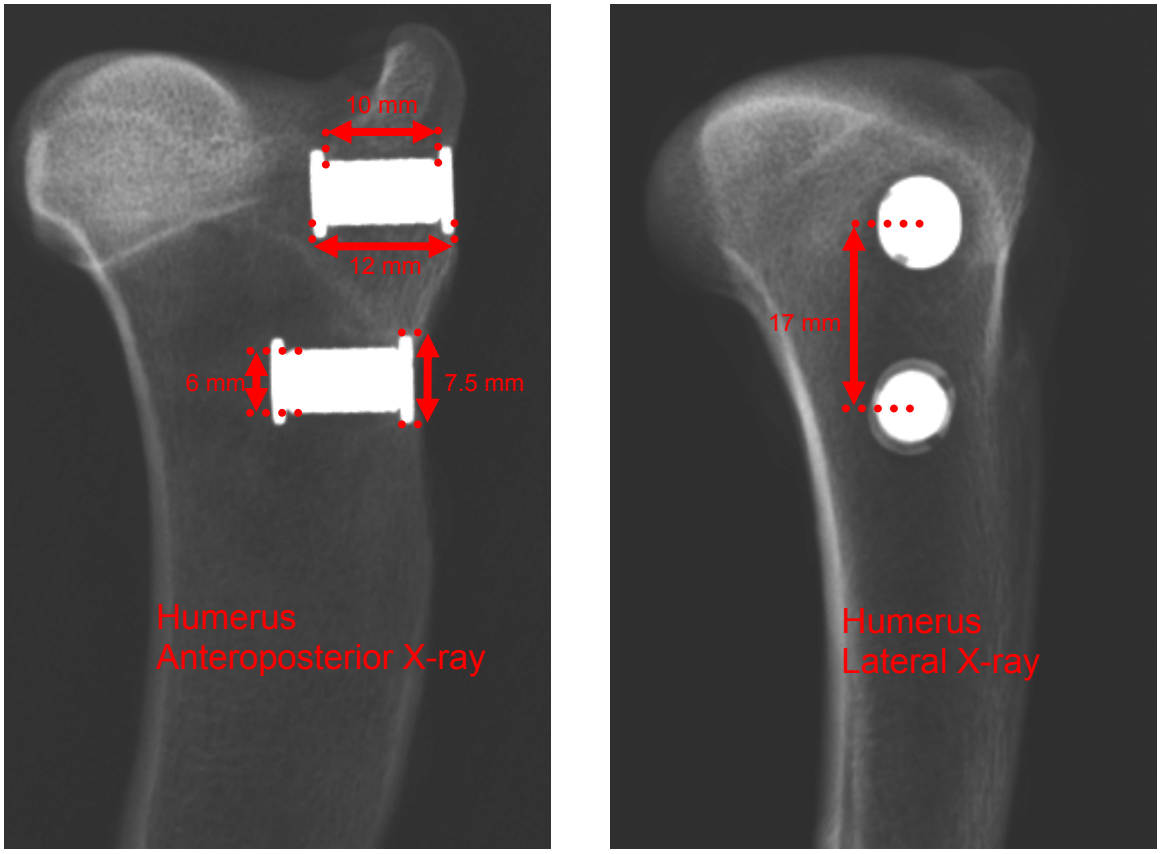

Figure 7. X-rays of implant positioning sites. The four implant types were inserted in the cancellous bone and systematically rotated between left, right, upper, and lower implant site (CoCrMo PoroCoat® and Titanium PoroCoat®).

Implants

CoCrMo PoroCoat® and Titanium PoroCoat® porous cylindrical implants (Depuy Inc., Warzaw, IN, USA) (L = 10 mm, Ø =6 mm) were used and specifications are listed in Table 4. The CoCrMo coating (beads) was as-cast CoCrMo.

Specimen preparation

After six weeks observation the animals were sacrificed with an overdose of hypersaturated barbiturate, and the proximal part of humerus was excised and cleaned and thereafter stored at –20°C. The outermost 0.5 mm of the implant-bone specimen was cut off and discarded. The

rest of the implant with surrounding bone was divided into two sections perpendicular to the long axis of the implant with a water-cooled silicon carbide cut-off wheel (Accutom – 50, Stuers A/S, Rødovre, Denmark). The outermost section was cut to a thickness of 3.0 mm and stored at –20°C pending mechanical testing [126]. The innermost section 6.5 mm was prepared for histomorphometri. The specimens were dehydrated in graded ethanol (70-100%) containing basic fucsin, and embedded in methylmetacrylate (Technovit 7200 VCL; Exact Apparatbau, Nordenstedt, Germany). Four vertical, uniform, random sections were cut with a hard-tissue microtome (KDG-95; MeProTech, Heerhugowaard, The Netherlands) around the centerpart of each implant, as described by Overgaard er al. [127], and parallel to the natural vertical axis of the implant. The 50-µm-thick sections were counterstained with 2% light green (BDH Laboratory Supplies, Poole, UK) and then mounted on glass [128]. Light green penetrates 5-10-µm into the tissue after 2-minutes exposure. This preparation provides red staining of non-calcified tissue and green staining of calcified tissues such as woven bone and lamellar.

Table 4. Implant specifications

Implant type	Coating Material	Porosity / Avg Pore size
CoCrMo Porocoat®	Spherical CoCrMo beads	40-50% / 250~300 µm
Titanium Porocoat®	Spherical CP Ti beads	40-50% / 250~300 µm

All CoCrMo substrates and beads were per ASTM F-1537. All Ti6Al4V substrates were per ASTM F-136. All Titanium beads were per ASTM F-67. All beads (Ti and CoCrMo) were attached by sintering process (heat/pressure in vacuum furnance). Courtesy of DePuy Inc., Warsaw, IN, USA.

Mechanical testing

Initial fixation is crucial for the long-term success of the implant [129,130]. In principle there are 3 destructive ways of testing the mechanical fixation of an implant: pulling, turning, and pushing the implant. All the methodologies have advantages; however, only one can be used because they are destructive. The torsion test resembles the stresses applied on a human implant, but it may be easier to standardize push-out than torsion test. Non-destructive test also exists, but requires many test subjects since many variables exists (different strain, Hz) [131].

Since the implant geometry was very alike in-between groups [132], implants were tested to failure by axial push-out test on a MTS Bionics Test Machine (Instrom Ltd., High Wycombe, UK). The specimens were placed on a metal support jig with a 7.4-mm diameter central opening. The implant was centralized over the opening thereby assuring a 0.7-mm distance between the implant and the support jig as recommended by Dhert et al. [133]. The direction of loading was from the cortical surface inward. A preload of 2 N was applied to standardize contact conditions before initiating loading. We used a displacement rate of 5 mm/min with a 2.5 kN load cell. Load and deformation were registered by a personal computer. Each specimen length and diameter was measured with a micrometer and used to normalize push-out parameters [125].

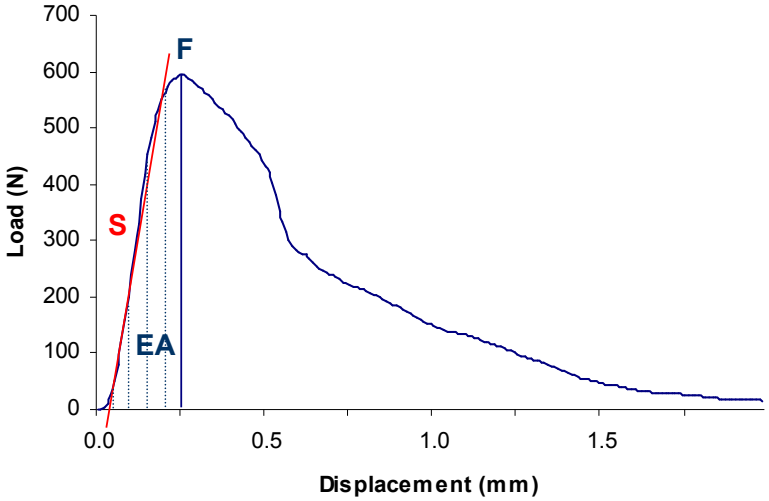

Figure 8. Load deformation curve. Ultimate shear strength (MPa) was determined from the maximum force (F) applied to the implant until failure. Apparent shear stiffness (MPa/mm) was obtained from the slope (S) of the linear part of the load displacement curve. Total Energy Absorption (EA) (J/m^2) was determined as the area under the load displacement curve until failure. All mechanical parameters were normalized by the cylindrical surface area of the implant section tested.

Ultimate shear strength (MPa) was determined from the maximal force applied until failure of the bone-implant interface.

$$USS\ (Pa) = F\ (N) / \pi dl\ (m^2)$$

USS – Ultimate Shear Strength, F – Maximum force, d – implant diameter, l – implant length

Apparent stiffness (MPa/mm) was obtained from the slope of the linear section of the curve.

$$S\ (Pa/mm) = \Delta(F/\pi dl)\ (Pa) / \Delta D\ (mm)$$

S – Apparent shear stiffness, D – Displacement

Energy absorption (J/m^2) was calculated from the area beneath the curve until failure.

$$EA\ (J/m^2) = \int_0^F LDC = \int_{D=0}^{D=F} f(D)\, dD$$

EA – Total Energy Absorption, LDF – Load Deformation Curve

Histological evaluation

Blinded histomorphometrical analysis was done using a stereological software program (CAST-grid Olympus Denmark A/S, Ballerup, Denmark). Fields of vision from a light microscope were captured on a computer monitor and a user-specified grid was superimposed on the microscopic fields. Four vertical sections representative of each implant were analyzed and cumulated [127,134]. Four requirements should be fulfilled when using the vertical sectioning technique; 1) A vertical axis of the specimen must be defined. 2) The specimen must be randomly rotated around its vertical axis before sectioning. 3) Histological sections must be made parallel to the axis. 4) A set of sine weighted isotropic uniform random (IUR) lines must be applied in the field of vision [135]. The specimen preparation procedure and the grid system made it possible to calculate unbiased estimates even though anisotropy in cancellous bone exists.

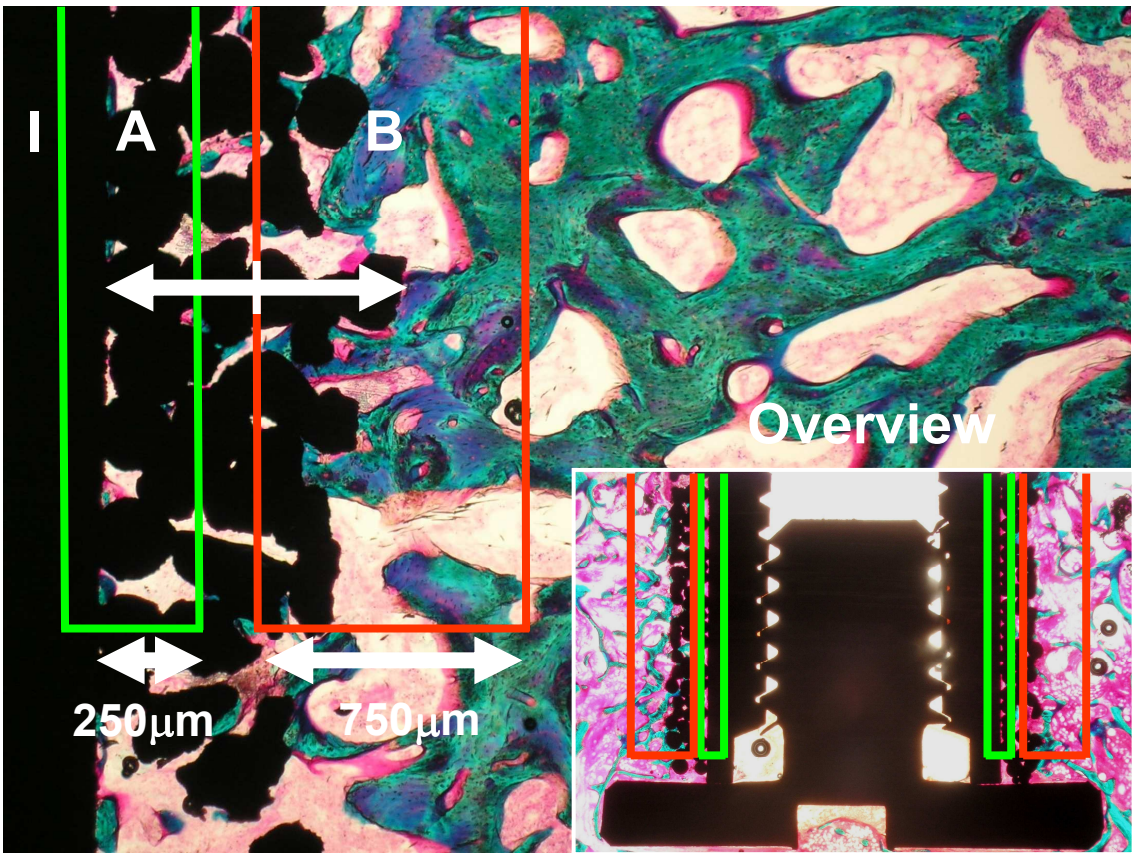

Figure 9. Regions of interest. Zone 1 (A) is defined as 250 µm from the implant (I) core surface and outwards. Zone 2 (B) is defined as a line between the core implant and "the outermost bead" and 750 µm outwards. The entire section with regions is presented in the overview.

With the aid of the software, we defined two regions of interest: a Zone 1 from implant core surface and 250 µm outwards, and a Zone 2 from a line between the core implant and "the outermost implant bead" and 750 µm outwards (Fig. 9). In Zone 1 and Zone 2 tissue-implant contact was defined as fraction of the implant surface covered with a particular tissue (bone, fibrous tissue, marrow space) and estimated using sine-weighted lines [134]. In Zone 2 tissue volume fractions were estimated by point counting [136,137].

Double measurements were carried out to calculate the intra-observer variation. The measurements were carried out by the same person using identical equipment and setup. The CE was calculated as: $S^2 = (1/(2k)) \Sigma d^2$ where k is the number of double measurements and d is

the difference between first and second assessment. Then *CV %* is calculated as: *CV % = (s/x) 100* where *x* is the mean value of the first and second assessment (Table 5).

Table 5: Reproducibility of histomorphometry. Variation Coefficient (CV %)

	Fibrous Tissue	New Bone	Marrow Space
Zone 1 (a)	*3 %*	*15 %*	*5 %*
Zone 2 (v)	*47 %*	*7 %*	*3 %*
Zone 2 (a)	*55 %*	*3 %*	*2 %*

All the variations are well below the expected range. The large CV% on fibrous tissue in Zone 2 is caused by a low absolute amount of fibrous tissue here. The very low CV% from Zone 1 confirms the fact that it is possible to readily identify fibrous tissue.
Sampling intensity was based on a rule-of thumb that any given tissue should be encountered on a minimum of 50 hits per implant (personal communication with Jens Nyengaard/Jørgen Baas). As previously described the total variation is mainly determined by the biological variance [135] and the "stereological" and "analytical" variance only plays a minor role as observed by the coefficient of variation. Confirming the rationality of the sampling intensity, coefficient of variation was, as mentioned before, well below the acceptable range (Table 5).

Statistics

Study I
Both PIXE results and MT-I/II mRNA transcription data were found not to fit normality of distribution. Non-parametric Kruskall-Wallis ANOVA test with Bonferoni correction for multiple comparison testing was used. A $p<0.05$ was considered significant. Results are given as median with interquartile range (IQR).

Study II
Both cytokine secretion and mRNA transcription data were found not to fit normality of distribution. Concentrations below the detection limit were expressed as one half of the method detection limit. Data were normalized to the mean of the control (control = 1), and non-parametric Kruskall-Wallis ANOVA test with Bonferroni correction for multiple comparison testing was used. A $p<0.05$ was considered significant. Results are given as median with IQR.

Study III
Cytokine secretion, mRNA transcription, and surface parameters were found not to be normal distributed. Non-detectable low results were assigned to 0 when calculating the statistic. Non-parametric Kruskall-Wallis ANOVA test with Student-Newman-Keuls correction for multiple comparison testing was used. A $p<0.05$ were considered statistically significant. Results are given as median with IQR.

Study IV
Histological and biomechanical data that followed a normal distribution and had equal variance were analyzed with 2-way ANOVA considering implant positioning (upper - lower) and group (CoCr PC and Titanium PC). A statistically significant extremely consistent difference existed between upper and lower implant position. Since the implants were systematically rotated no bias was introduced, and the 2-way ANOVA helped to reduce that source of variation. When a statistically significant difference was found between the groups, a

Student's paired t-test comparison of the groups followed. The data were presented as means with 95% confidence intervals (CIs), and p-values less than 0.05 were considered statistically significant.
Data that did not fulfill the assumptions for 2-way ANOVA were analyzed with a Wilcoxons signed rank test comparison of only the groups. The data were presented as medians with IQR, and p-values less than 0.05 were considered statistically significant.

Ethical consideration

There is no alternative to large animal experiments at this late stage of the investigation of the implant properties. Canines are used, as they represent human bone best. In study I Wistar rats were used because of ethical considerations with larger animals, in particular since no obvious advantage exist when extrapolating the results to human setting. Both study I and study II were approved by the Animal Experiments Inspectorate under the Danish Ministry of Justice.

Results

Metal release from CoCrMo implants - Accumulation in kidney and liver (Study I)

PIXE analyses

The levels of Mo, Si, P, and S were increased in both kidney and liver (Table 6) of rats exposed to CoCrMo alloy intramuscularly. Liver accumulation of Cr and Mn were also found as well as increased kidney levels of Ca and Zn. Intraperitoneal exposure to the identical concentrations of CoCrMo alloy did not result in any statistically significant changes compared to control animals.

Table 6. Metal concentration in parts per million (PPM).

	Intraperitoneal exposure	**Intramuscular Exposure**	**Control sham operated**
Cobalt			
Liver	0.27 [-0.13,0.35]	0 [0,0]	0 [0,0]
Kidney	1.00 [0.83,1.07]	1.16 [0.84,1.90]	1.20 [0.58,1.36]
Chromium			
Liver	1.27 [0.99,1,41]	2.12 [1.89,2.44] *****	1.37 [1.20,1.74]
Kidney	2.76 [2.01,3.29]	3.10 [2.38,3.71]	2.47 [2.36,2.78]
Molybdenum			
Liver	1.96 [1.88,2.23]	3.40 [3.03,4.03] *****	2.10 [1.92,2.42]
Kidney	1.41 [1.16,1.94]	1.87 [1.66,2.05] ◊	1.28 [1.20,1.47]
Manganese			
Liver	8.17 [7.31,8.83]	9.39 [8.67,9.72] ●	8.54 [7.45,8.73]
Kidney	3.70 [3.48,4.02]	3.99 [3.96,4.14]	4.19 [3.87-4.63]
Silicon			
Liver	636 [608,664]	731 [701,800] *****	632 [586,674]
Kidney	931 [768,1051]	1041 [951,1090] ◊	888 [856,933]
Nickel			
Liver	0.32 [0.28,0.40]	0.53 [0.37,0.65]	0.63 [0.57,1.39]
Kidney	0.54 [0.46,1.06]	0.81 [0.70,1.29]	0.71 [0.63,1.19]
Phosphate			
Liver	8960 [8927,9169]	10247 [9459,10405] *****	8680 [8521,9042]
Kidney	11511 [10444,13180]	12470 [11823,14023] ◊	10771 [10398,11124]
Sulfur			
Liver	7426 [7361,7968]	8505 [7819,8727] ◊	7508 [7229,7723]
Kidney	10298 [8865,10808]	11148 [10550,11887] ◊	9802 [9392,10015]
Chloride			
Liver	2216 [2032,2321]	2478 [2113,2730]	2000 [1800,2345]
Kidney	6584 [6318,7170]	6824 [5434,7738]	5763 [5409,5858]
Calcium			
Liver	154 [145,162]	160 [151,175]	162 [149,174]
Kidney	449 [407,549]	3594 [633,5954] *****	449 [444,475]
Zink			
Liver	98.0 [92.4,100]	98.5 [93.8,103]	96.2 [91.9,101]
Kidney	89.9 [86.9,97.6]	124 [116,136] *****	98.8 [93.6,106]

Metal concentration in 60 µm thick liver and kidney tissue sections. PIXE results are normalized to potassium concentration which is assumed to a constant within tissue. [*****: $p<0.05$ vs. IP and Control; ◊: $p<0.05$ vs. Control; ●: $p<0.05$ vs. IP; median with IQR, n=9, 9, 9]

Metallothionein I/II mRNA expression

MT-I/II in liver tissue was expressed at a higher level when rats were exposed to CoCrMo IM (1.4 MT-I/MT-II mRNA relative to HKG index [0.6-4.2] vs. 0.45 MT-I/MT-II mRNA relative to HKG index [0.3-0.7] and 0.55 MT-I/MT-II mRNA relative to HKG index [0.3-1.2], p>0.05). No difference in mRNA transcription in the kidneys was seen (Fig. 10).

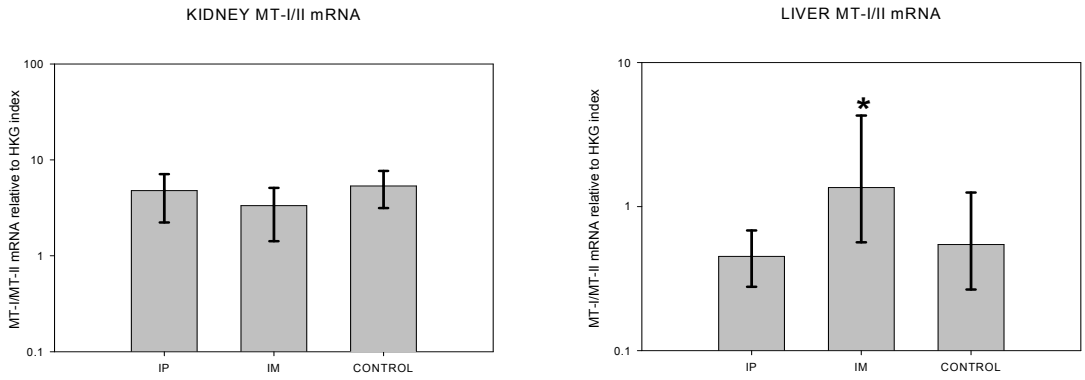

Figure 10. Metallothionein-I/II (MT-I/II) mRNA relative to housekeeping index (HKG) in kidney and liver tissue. Rats have had a 20-cm long and 0.1001-mm thick coiled piece of ASTM F75 CoCrMo wire implanted either intraperitoneally (IP), intramuscularly (IM), or sham operated as control. [* : p<0.05 vs. IP, Median with IQR, n=9, 9, 9]

Weight of Wistar rats

All animals survived the surgical procedure, and were observed for signs of pain and malnourishment daily in the entire observation period. No deviations were detected. At the beginning of the observation period no difference between weights of the animals was observed; however, before sacrificing the weight gain of the IM implanted group was significantly reduced compared to IP implanted and control group (379.1g ± 35.5g vs. 483.6g ± 12.4g and 469.3g ± 12.5g, p<0.05) (Fig. 11).

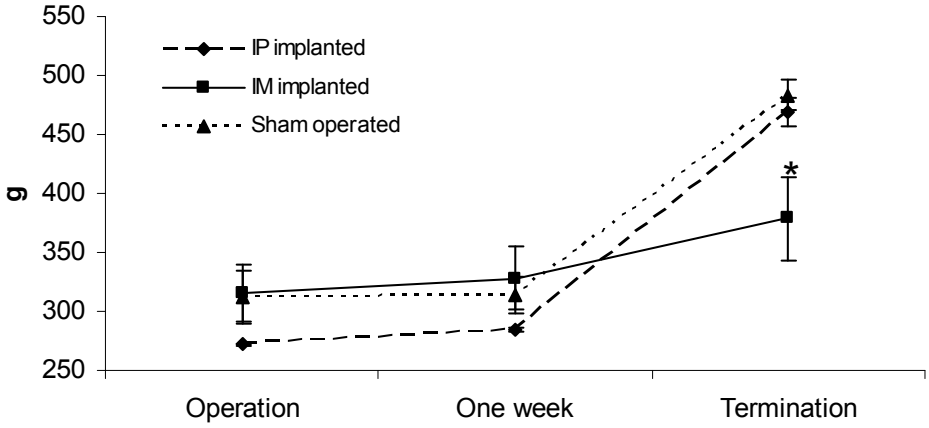

Figure 11. **Weight of the Wistar rats.** Animals received either a CoCrMo wire implanted intraperitoneally (IP), intramuscularly (IM), or received a sham operation (control). At the beginning of the observation period and at one week no differences between the groups appear. Prior to sacrificing after 9 month the IM implanted group exhibit a reduced growth rate (p<0.05). [* : p<0.05 vs. IP and sham operated.]

CoCrMo and TiAlV (Study II)

Pro-inflammatory response

Protein secretion (TNF- α, IL-6, IL-1α, and IL-1β) was not affected by the type of prosthetic material. When pooling data from all exposed cell cultures a significant 11-fold – 300-fold increase compared to the secretion from non-stimulated cells was seen (Fig. 12). Cells culture exposed to as-cast HC CoCrMo demonstrated a significant (p=0.029) suppression of IL-6 mRNA compared to TiAlV (Fig. 13A). The reduction observed for as-cast HC CoCrMo was 77 % compared to the rest of the alloys. The pro-inflammatory mRNA (TNF- α, IL-6, IL-1α, and IL-1β) was otherwise not affected by alloy type. When pooling data from all exposed cell cultures a significant 3-fold – 130-fold mRNA increase compared to non-stimulated cells was seen.

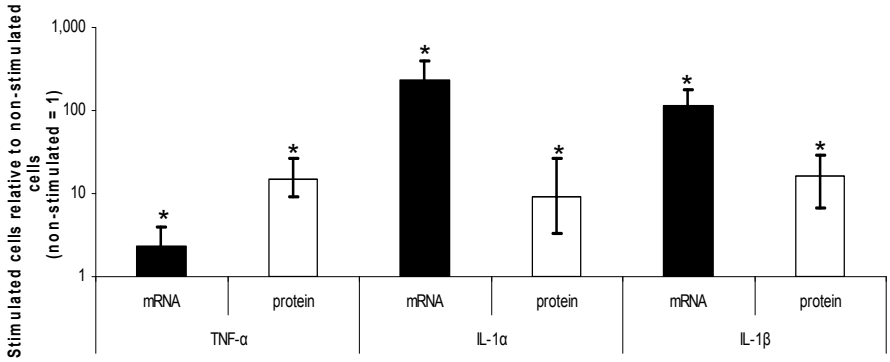

Figure 12. Pooled data between all the different alloys (wrought HC CoCrMo, wrought LC CoCrMo, as-cast HC CoCrMo and wrought TiAlV). Data are shown relative to non-stimulated cells. (Median with IQR; *: p<0.01 vs. non-stimulated cells, n=40)

Chemokine response

MCP-1 protein secretion was statistically significantly reduced by 36 % when cells were incubated with as-cast HC CoCrMo compared to secretion from wrought HC CoCrMo, wrought LC CoCrMo, and TiAlV (p<0.05). Pooling data from all materials showed a 7.3-fold mRNA increase compared to non-stimulated cells (p<0.01), but it was not suppressed by as-cast HC CoCrMo (Fig. 13B).

Proliferative response

M-CSF protein secretion was significantly reduced by 62 % when cells were incubated with as-cast HC CoCrMo compared to the pooled secretion from wrought HC CoCrMo, wrought LC CoCrMo, and TiAlV (p<0.01). Pooled data from wrought HC CoCrMo, wrought LC CoCrMo, and TiAlV were 13-fold increased compared to non-stimulated cells. Pooled mRNA data from all the different alloys exhibited a 2.6-fold increase compared to non-stimulated cells (p<0.01), but it was not suppressed by as-cast HC CoCrMo (Fig. 13C).

Bone-conserving response

The protein secretion of OPG and IL-10 was undetectable low. OPG and IL-10 mRNA was modestly reduced by 0.85-fold – 0.43-fold compared to non-stimulated cells, but this did not reach statistical significance. TGF-β protein levels were not affected by implant material. TGF-β mRNA was modestly reduced by to 70% of the level in non-stimulated cells, but this did not reach statistical significance.

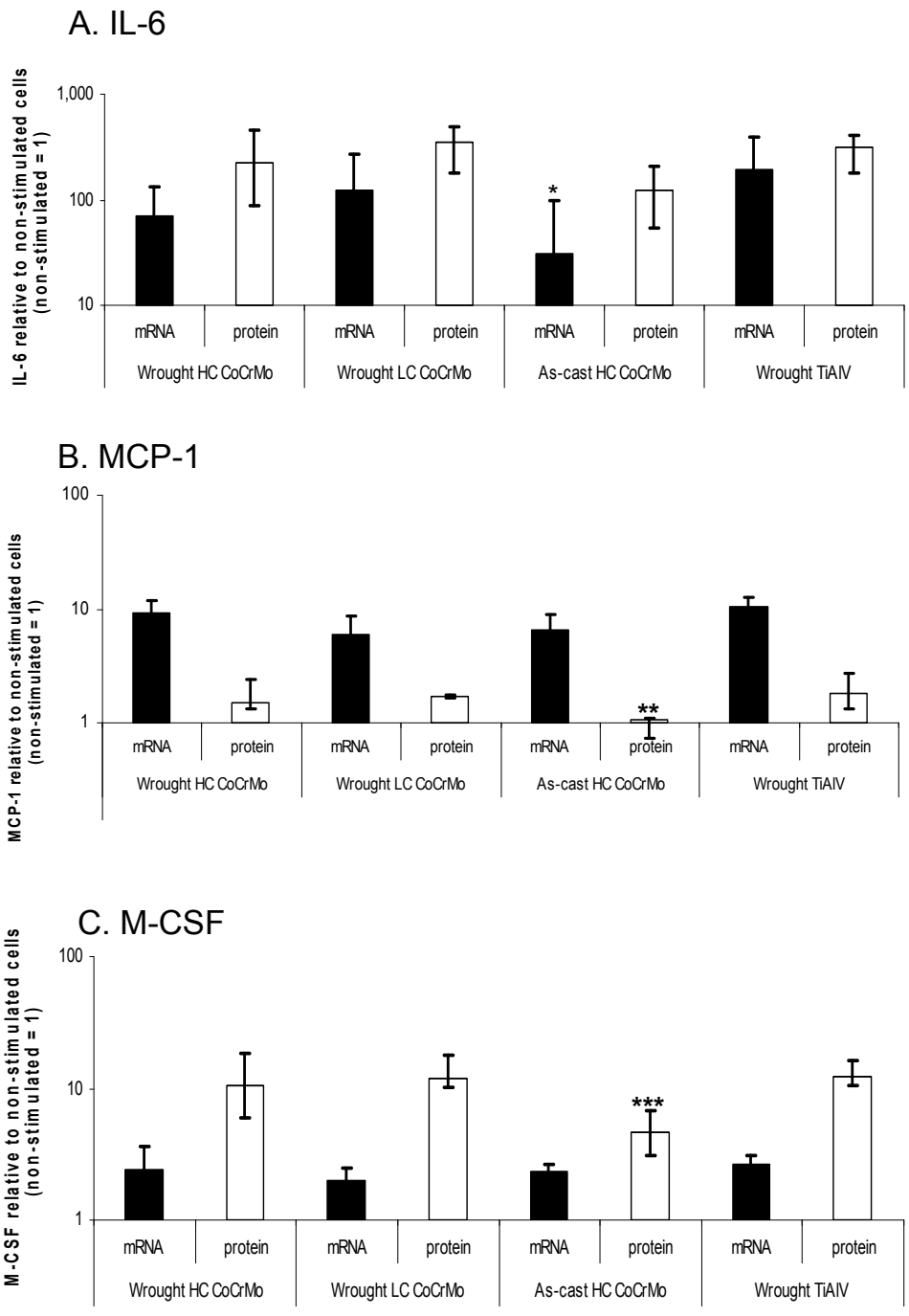

Figure 13. IL-6 (A), MCP-1 (B), and M-CSF (C) protein secretion and mRNA transcription from J774A.1 macrophages. Cells were incubated with the different prosthetic alloys, and secretion and transcription is presented relative to non-stimulated cells (Median with IQR; *: p = 0.029 vs. wrought TiAlV, **: p<0.05 vs. wrought HC CoCrMo, wrought LC CoCrMo, and wrought TiAlV, ***: p<0.01 vs. wrought HC CoCrMo, wrought LC CoCrMo, and wrought TiAlV, n=10).

Plasmaspray- and porouscoating ±HA (Study III)

Pro-inflammatory response

HA increased the TNF-α protein secretion from J774A.1 macrophages. Plasmaspray titanium discs + HA increased the TNF-α secretion with 150% after 6 hours and 300 % after 24 hours compared to - HA discs ($p<0.05$). Porous coated titanium + HA elicited the same pattern, 75% and 230 % increase after respectively 6 and 24 hours ($p<0.05$).

HA increased the IL-6 protein secretion from J774A.1 macrophages; however, only at very low levels. Plasmaspray discs + HA increased the IL-6 protein secretion with 230 % after 24 hours compared to – HA discs ($p<0.05$). Porous coated titanium + HA elicited a different pattern. After 6 hours a 70 % decrease was observed, but after 24 hours an 88 % increase was observed ($p<0.05$) (Fig. 14).

Bone generating response

Pre-activating the J774A.1 macrophages increased the TGF-β secretion statistically significant when incubated with plasmaspray disc ± HA ($p<0.05$). HA did not statistically significant affect TGF-β secretion or transcription; however, a tendency towards a HA suppressing effect was observed after 24 hours.

Activated cells incubated with plain titanium discs expressed the lowest levels of BMP-2, and with both activated and non-activated cells HA increased the BMP-2 expression. But HA did not statistically significant affect BMP-2 secretion or transcription after 24 hours incubation. Non-activated cells without plasmaspray discs expressed the highest median level of BMP-2 (Fig. 15). The protein secretion of BMP-2 was found undetectable low in all groups.

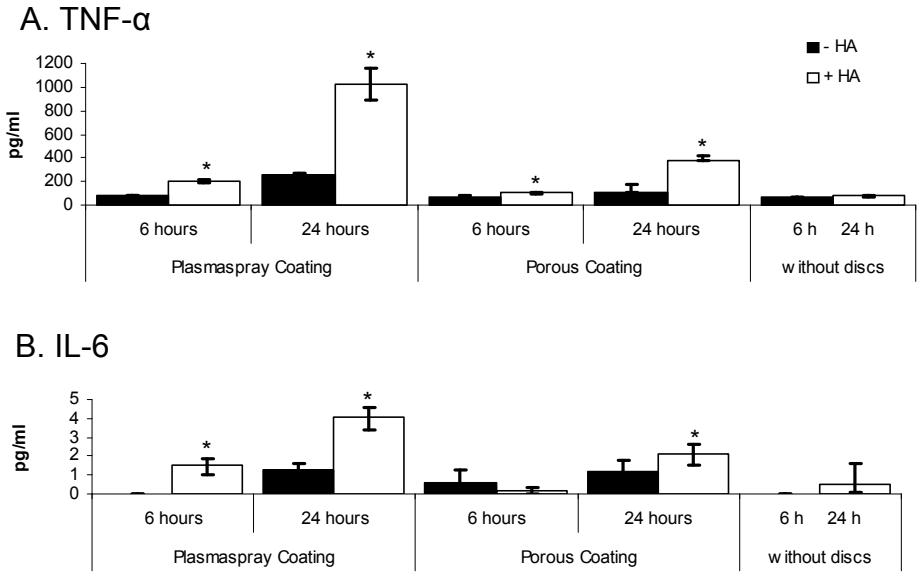

Figure 14. Macrophage J774A.1 TNF-α and IL-6 secretion when incubated with discs. A. TNF-α protein secretion from cells incubated 6 or 24 hours with plasmaspray and porous coated discs ± hydroxyapatite (HA) and non-stimulated cells. B. IL-6 protein secretion from cells incubated 6 or 24 hours with plasmaspray and porous coated discs ± HA, and cells grown without discs.

Cytokine levels in culture supernatants were determined with ELISA assays, and data are presented as median with IQR (*: p<0.05 vs. - HA).

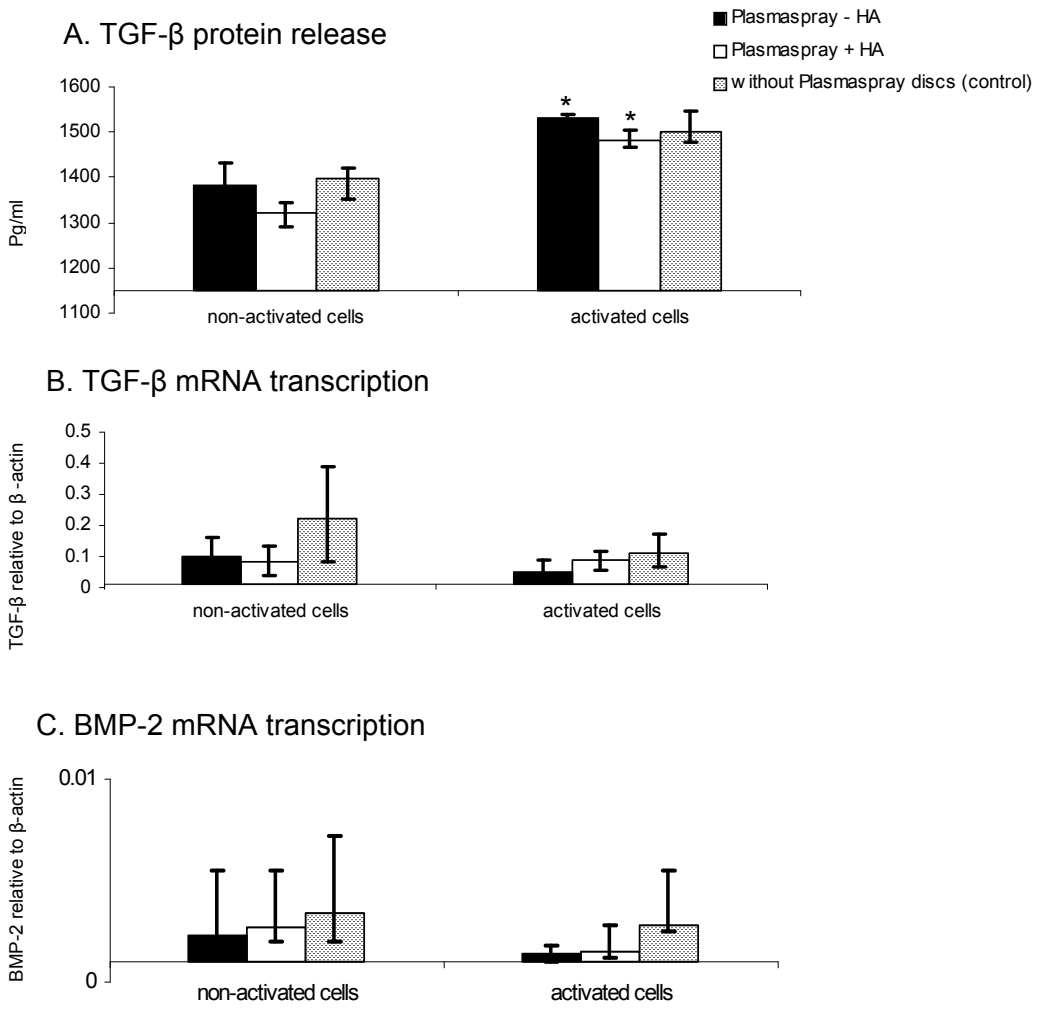

Figure 15. Macrophage J774A.1 TGF-β and BMP-2 release. A) TGF-β protein secretion from cells incubated 24 hours with plasmaspray coated discs ± hydroxyapatite (HA), and cells grown without the presence of a Plasmaspray disc. B) TGF-β mRNA release from cells incubated 24 hours with plasmaspray coated discs ± HA, and cells grown without discs. C) BMP-2 mRNA release from cells incubated 24 hours with plasmaspray coated discs ± HA, and cells grown without discs. Cytokine protein levels in culture supernatants were determined using ELISA assays and mRNA levels were determined with real time RT-PCR. Data are presented as median with IQR. (*: p<0.05 vs. Plasmaspray ± HA incubated with non-activated cells)

CoCrMo impact on osseointegration (Study IV)

Mechanical results

Both implant groups were well anchored in the bone, but the Titanium PC implants had better mechanical fixation than the CoCrMo implants in all parameters (Table 8).

Table 8. Biomechanical Implant Fixation

Biomechanical Parameters	Maximum shear strength (MPa)	Total energy absorption (kJ/m^2)	Maximum shear stiffness (MPa/mm)
CoCrMo PC	2.37 [1.50 – 3.24]	0.33 [0.19 – 0.57]	12.14 [7.20 – 17.08]
Titanium PC	4.15 [2.48 – 5.82]	0.51 [0.36 – 0.84]	21.61 [12.34 – 30.88]
	Parametric data, p=0.04	*Parametric data, p=0.01*	*Parametric data, p=0.04*

Parametric data are presented as mean with 95% CI. Non-parametric data are presented as median with interquartile range. n=10.

Histomorphometry results

The formation of new bone in the gap was comparable between the implants, and almost no fibrous tissue was formed (Zone 2). We observed a tendency towards decreased bone tissue coverage in Zone 1 for Titanium implants. Results from histological analysis are seen in Table 7).

Table 7. Histomorphometry results

	Bone (New)	Fibrous Tissue
Zone 1 (-250 µm - 0)		
Area fractions in percent.		
CoCrMo PC	6.8 [3.5 – 10.1]	64.7 [52.5 – 76.9]
Titanium PC	4.3 [1.8 – 7.5]	71.8 [57.5 – 86.1]
	Parametric data, p=0.10	*Parametric data, p=0.26*
Zone 2 (0 – 750 µm)		
Area fractions in percent.		
CoCrMo PC	15.6 [10.6 – 20.6]	1.9 [1.0 – 4.6]
Titanium PC	16.2 [11.2 – 21.2]	2.5 [1.4 – 13.7]
	Parametric data, p=0.93	*Non-parametric data, p=0.63*
Zone 2 (0 – 750 µm)		
Volume fractions in percent.		
CoCrMo PC	18.2 [12.5 – 23.9]	0 [0 – 0.2]
Titanium PC	21.0 [13.8 – 28.2]	0.2 [0 – 2.2]
	Parametric data, p=0.57	*Non-parametric data p=0.20*

Parametric data are presented as mean with 95% CI. Non-parametric data are presented as median with interquartile range. n=10.

Discussion

The aim of these studies was to evaluate biocompatibility of CoCrMo alloy, and the results and methods used will be discussed in relation to the relevant literature.

Metal release from CoCrMo implants - Accumulation in kidney and liver (Study I)

Molybdenum and silicon accumulated in both kidney and liver, while chromium and manganese collected in the liver only. Increased levels of metallothioneins were recorded exclusively in the liver.

These differences are not easily explained, but must be based on different metabolic routes of pacifying/detoxifying the individual metal. AMG traceable metal ions have been found to accumulate in lysosomes of certain cells, i.e., it is not all cells that take up these metal ions [138,139], and recently kupffer cells in the liver have been suggested to play a central role in removal of nanoparticles from the organism [140]. This phenomenon does not reveal the nature of possible damages that the metal ions might cause the cells, but it certainly marks the cells that are influenced by the pollution.

When we removed the implants they were all, independent of the site of implantation, covered by a whitish layer of granulation tissue which contains many macrophages. From our knowledge of how gold and silver implants releases gold respectively silver ions by a process where macrophages act as dissolucytes and dissolve the metals into the dissolution membrane, we feel confident that the released metal ions in this study are liberated by the same mechanism [21,22]. We do not expect any release of nanoparticles from the implants as no mechanical wear takes place in this experimental model. However, such nanoparticles are known to be released from human prosthetic devices, where they are taken up by macrophages and other cells by endocytosis. Metal nanoparticles are largely contained in the lysosomes of macrophages where the dissolucytotic process does not take place and therefore is believed not to give rise to release of metal ions [140].

We hypothesize that the evident release of metal ions from the intramuscularly placed implants as compared to the implants placed in the abdomen is caused by the muscle having a much higher metabolic turnover. This will cause a far more intense local inflammation in the muscle as compared to the peritoneum [141]. The mechanical movement of the implant at every contraction of the muscle will further stimulate the process. A previous report corresponds well with our results showing that intramuscularly metal implants liberates metal ions to the surrounding tissue [142].

Kidney and liver were chosen as target organs because these organs are known to be involved in the excretion of many metals (e.g. gold, silver, mercury, and bismuth), and the multi-element approach, Proton Induced X-ray Emission, PIXE, were chosen to ensure that possible changes in the normal metal pattern were recorded along with the foreign metals [105,106,143].

The observed statistically significant increase in MT-I/II mRNA expression in the liver of IM implanted animals and the lack of differences between groups, however still high expression in the kidneys, corresponds well to the fact that MT-I/II is mainly produced in the liver and kidney. The metallothionein gene expression is induced by a variety of stimuli, as metal ion exposure (Zn, Cu, Cd, Hg), oxidative stress, glucocorticoids, catecholamine's, ROS, hydric stress, lipopolysaccharide (LPS), physical and physiological stress [144,145]. The possibility that one or more of the liberated metal ions (Co, Cr, Mn, Fe, and Ni) originate the increased expression in the liver is tempting, but we simply don't know at the moment [146-148].

Macrophage cytokine response to CoCrMo (Study II and III)

We here report that implant surface (non-phagocytosable) induces a substantial pro-inflammatory response regardless alloy type and surface topography. As-cast HC CoCrMo; however, reduces the mouse J774A.1 IL-6 transcription, MCP-1 protein secretion, and M-CSF protein secretion by 77%, 36 %, and 62 %, respectively. Furthermore, when the biocompatibility of commercially available 3D-surfaces was improved by plasma sprayed hydroxyapatite the pro-inflammatory response [TNF-α, IL-6] was statistically significant increased more than 100 %.

IL-6, MCP-1, and M-CSF are important proteins in relation to regulation of ostesclasts (Fig. 1). Osteoclasts are the final common pathway in osteoloysis, and bone resorption is dependent on number, activity, and survival of osteoclasts. It has been proposed that TiAlV induce higher IL-6 secretion as compared to CoCrMo, whereas CoCrMo alloys induce higher TNF-α secretion [76]. This distinction has previously been reported in RAW 264.7 cell [149]. In line with these findings, we found TiAlV to reduce TNF-α secretion by ~50% compared to CoCrMo alloys, and TiAlV to increase IL-6 secretion by ~100% as compared to as-cast HC CoCrMo. As opposed to Sethi et al. using both wrought and as-cast CoCrMo, we observed that only as-cast CoCrMo suppressed IL-6 compared to TiAlV, but the increase in TNF-α was seen for both wrought and as-cast CoCrMo alloys. TNF-α, IL-1α, and IL-1β increase osteoclast survival rate [86], transforms osteoclast precursors to mature osteoclasts [87], and activates resident non-activated osteoclasts [88,91,96]. Wear particles are strongly correlated to aseptic loosening, but in line with Sethi et al. [149], we observed a large statistically significant increase in TNF-α, IL-6, IL-1α, and IL-1β transcription and secretion from cells incubated with discs (pooled data from all the different alloys) (Fig. 12 and Fig. 13) compared to non-stimulated cells. These findings can be explained by that macrophages express and secrete cytokines independently of the internalization process [71-73].

Prosthetic surface structure (porosity, surface roughness) influences osteointegration and prosthetic fixation greatly [150]. Surfaces also influence immunoactive cells as macrophages. We did not find any differences in the pro-inflammatory response between polished and rough discs in study II; both rough and smooth as-cast discs were able to suppress IL-6, MCP-1, and M-CSF. Macrophages cultured on a rough surface together with mouse calvarias show increasing ^{45}Ca immersion compared to macrophages cultured on a smooth surface [151]. The specific relationship between surface topography, inflammation, and tissue regeneration has not yet been established, but it has been suggested that roughened surface influence macrophage adhesion, proliferation, and activation [70]. Between CoCrMo alloys the atomic composition are very alike. When trying to explain the observed suppression, the possibility of an unknown third factor in the macrophage – surface interaction must be considered. In as-cast CoCrMo carbide structures are more roughly dispersed in the alloy compared to wrought CoCrMo a potential origin of different ion release profile [10]. Ion flow channels are hypothesized [152] to exist close to the blocky carbides sticking out of the surface oxide layer, and these carbides are seen in as-cast CoCrMo though the theory is still much debated [153].

In the initial phase of implantation it is not obvious that early suppressing effects on M-CSF, IL-6, and MCP-1 is advantageous. In the reparative phase chemokines, pro-inflammatory, and proliferate cytokines are important mediators in normal wound healing in bone. Another picture could be seen in the long run, where a chronic foreign body reaction could be avoided by a very low stimulating effect of the implant material. The pro-inflammatory response [TNF-α, IL-6] was statistically significant increased for both plasmaspray- and porouscoated discs with hydroxyapatite compared to discs without hydroxyapatite.

Mesenchymal stem cells cultured with medium from non-stimulated J774A.1 cells increase alkaline phosphatase secretion, which can be blocked by anti-BMP-2 and anti-TGF-β1. The

increase in alkaline phosphatase could also be blocked or decreased by treating the J774A.1 with LPS (correlated to TNF-α) [112,114]. This corresponds well with our BMP-2 findings where HA coated plasmaspray discs activated macrophages, and only very low levels of BMP-2 transcription were observed. However, LPS activated cells transcripted an even lower level of BMP-2. Opposite to these results, we observed that TGF-β protein secretion increased when cells were LPS activated. TGF-β1 and TGF-β2 has previously been found elevated in capsule and pseudocapsule in patients with a loose prosthesis, potentially secreted by activated macrophages [154]. In study II, bone conserving cytokine transcription was reduced by 54 % (IL-10), 15% (OPG), and 30% (TGF-β) for pooled data of all CoCrMo and TiAlV discs compared to non-stimulated cells. But none of the reductions were statistically significant.

Recently, it has been shown that macrophages incubated with HA coated (anodic oxidation and hydrothermal treatment) discs increases transcription and secretion of BMP-2 compared to smooth commercial pure Titanium [112]. We did not observed the same increase in BMP-2 most likely because commercial 3D-surfaces activates the macrophages more and thereby decreasing the BMP-2 production. It has been reported that small and needle shaped HA particles activate human monocytes and induces an increase in TNF-α, IL-6, and IL-10 [155]. As opposed to our results only a very low stimulatory effect of non-phagocytosable sizes were found in that study. Increasing the surface area ratio (SAR) 10-fold increased TNF-α and IL-6 production to a level comparable with our findings for non-phagocytosable sized HA [156]. Using 3D-surfaces increase the SAR compared to more simple surface topographies presenting a likely explaining for these differences. Furthermore, needle shaped particles induced the highest levels of TNF-α and IL-6 production possible analogue to our finding, where the more spiky plasmaspray coated discs induced a higher pro-inflammatory level compared to the porous coated discs. All though hydroxyapatite effects on cytokine production are many-sided hydroxyapatite clearly has the potential to play an active role in the bone remodeling through macrophages cytokine production, and not only acting as a passive scaffold and inert surface for osteoblasts. The functional mechanism for hydroxyapatite on orthopedic devices is believed to be due to: 1) increased absorption of cell adhesion proteins and local growth factors, 2) osteoconduction, and 3) dissolution and re-precipitation of natural bone-like matrix [157].

CoCrMo impact on osseointegration (Study IV)

We found a statistically significant decrease ($p<0.05$) in biomechanical fixation for CoCrMo PoroCoat® compared to Titanium PoroCoat® but with comparable histological parameters.

Dissoluted metal ions from the implant surface are known to affect peri-implant cells in particular osteoblast [22,23]. MG-3 osteoblast, fibroblasts, and lymphocytes proliferation are susceptible to metal ions in particular Vanadium, Nickel, and Cobalt [99]. Apoptosis and/or necrosis are induced in a wide range of cells by metal ions liberated from implant material [100]. Released Co and V are more cytotoxic [18], than Al, Fe, Cr, and Mo; however, these ions seems to suppress osteoblast proliferation more than fibroblasts proliferation [99]. Furthermore, it has been demonstrated that osteoblasts grow faster on Titanium-alloy than on CoCrMo-alloy [158]. Based on those results, an expected outcome would be inferior performance of CoCrMo implants compared to Titanium-alloy implants.

We found that the mechanical fixation of the CoCrMo implants was poorer than the Titanium implants, but bone to implant contact was comparable. This coheres with previous reports where only mechanical fixation, and not osseointegration, was affected by CoCrMo [159]. The lack of difference in terms of bone-implant contact and peri-implant bone volume could be explained by either a decreased intimate bone-implant adhesion on a submicroscopic level, or

by a decreased bone quality. Secretion of extracellular matrix proteins and mineralization has previously been shown to be decreased by CoCrMo alloy compared to Titanium potentially creating a weak bone quality and/or bone-implant interface [160]. Moreover, the released levels of metal ions may be too low to induce detectable changes in bone density but large enough to affect the bone-implant interface or the bone quality. Previously, research has suggested that a threshold level must be reached (Co – 0.8 mM for both fibroblasts and osteoblasts; V – 0.1 mM respectively 0.4 mM) to negatively influence cells [99].

If a significant metal-ion concentration gradient from the implant and outwards existed, we would expect that, fibrous tissue area-fraction would increase and bone tissue area-fraction would decrease in the deep porosity. We observed a tendency towards decreased bone tissue coverage in Zone 1 for Titanium implants. This may reflect the fact, that substrate implant are made of TiAlV alloy potentially releasing V and Al with negative effects on peri-implant cells [99]. Moreover, in both groups, less bone tissue (area-fraction), and more fibrous tissue were detected in Zone 1 compared to Zone 2 ($p<0.01$, two-way ANOVA) which may also be a sign of a concentration gradient.

Conclusion and perspective

Insertions of CoCrMo implants are associated with a disturbance of the delicate peri-implant milieu. Even from implants not subjected to any mechanical forces, metal ions are 'dissoluted' by macrophages and result in intra- and extracellular accumulation in the immediate implant vicinity [21,22,107]. Metal protection protein Metallothionein was up-regulated in liver perhaps as a response to this metal ion exposure.

Macrophages exposed to CoCrMo metal discs did not significantly increase the pro-inflammatory response, actually IL-6 expression, and MCP-1 and M-CSF secretion decreased when exposed to as-cast high carbon CoCrMo alloy. Furthermore, adding plasmasprayed hydroxyapatite on commercially available 3D-surfaces statistically significant increased the pro-inflammatory response indicating that pro-inflammatory macrophages response may not always be caused by of lack of biocompatibility.

The short-term biocompatibility was affected, and mechanical implant fixation was decreased compared to Titanium implants. Implant osseointegration was comparable between the two implants; however, a slight decrease in bone volume density around CoCrMo implants was observed.

The long-term biocompatibility is still to be revealed; however, a continuous burden of wear particles and metal ions should be encountered, and theoretically many untoward effects may exist. Epidemiological studies raise questions of a moderate increased risk of melanomas, cancers of the urinary tract and in oropharynx [32]. A possible causal relation is yet to be discovered.

Suggestions for future research

In the clinical setting, with CoCrMo implants, bulk material, nano wear particles, and raised ion levels are unavoidable. Both the initial osseointegration and the late bone remodeling in relation to implants may be affected by the alloy. In clinical practice, a small, but mechanically very important portion (10% to 20%) of the un-cemented press-fit implant surface is in bone contact [161]. We believe, that an implant's ability to provide early, stable and osseous fixation is important and predictive of implant survival, as indicated by numerous radio stereometric analysis studies. Respective of this, our results show that CoCrMo may be inferior to titanium. However, the material composition of an implant also determines other important properties such as elastic modulus and wear resistance, which are not subject to evaluation in this model. The choice between titanium alloy and CoCrMo should ultimately be governed by a comprehensive review of all factors influencing clinical implant survival.

Additionally, the impact of a continuously exposure of metal ions, metal particles, and metal surfaces on osteoblasts and mesenchymal stem cells could be of great importance and needs further clarifying.
Long-term biocompatibility is controversial, macroscopically and microscopically (molecular) mapping of the metal ions and wear particles can be used to address the potentially negative impact on the affected tissue and molecules.

Reference List

1 Pedersen AB, Johnsen SP, Overgaard S, Soballe K, Sorensen HT, Lucht U. Total hip arthroplasty in Denmark: incidence of primary operations and revisions during 1996-2002 and estimated future demands. Acta Orthop 2005;76:182-189.

2 Lucht U. The Danish Hip Arthroplasty Register. Acta Orthop Scand 2000;71:433-439.

3 Malchau H. The Swedish Total Hip Replacement Register. Herberts P ETGGSP, editor. 84-A Suppl 2[J Bone Joint Surg Am], 2-20. 2002.

4 Malchau H. Prognosis of total hip replacement in Sweden. Herberts P AL, editor. 64[Acta Orthop Scand], 497-506. 1993.

5 Larsen A, Stoltenberg M, Danscher G. In vitro liberation of charged gold atoms: autometallographic tracing of gold ions released by macrophages grown on metallic gold surfaces. Histochem Cell Biol 2007;128:1-6.

6 August AC, Aldam CH, Pynsent PB. The McKee-Farrar hip arthroplasty. A long-term study. J Bone Joint Surg Br 1986;68:520-527.

7 Dorr LD, Long WT, Sirianni L, Campana M, Wan Z. The argument for the use of Metasul as an articulation surface in total hip replacement. Clin Orthop Relat Res 2004;80-85.

8 Schweizer A, Luem M, Riede U, Lindenlaub P, Ochsner PE. Five-year results of two cemented hip stem models each made of two different alloys. Arch Orthop Trauma Surg 2005;125:80-86.

9 Schweizer A, Riede U, Maurer TB, Ochsner PE. Ten-year follow-up of primary straight-stem prosthesis (MEM) made of titanium or cobalt chromium alloy. Arch Orthop Trauma Surg 2003;123:353-356.

10 Nevelos.J, Shelton.J.C., Fisher.J. Metallurgical considerations in the wear of metal-on-metal bearings. HIP Int 2004;14:1-10.

11 Chan FW, Bobyn JD, Medley JB, Krygier JJ, Tanzer M. The Otto Aufranc Award. Wear and lubrication of metal-on-metal hip implants. Clin Orthop Relat Res 1999;10-24.

12 Firkins PJ, Tipper JL, Saadatzadeh MR, Ingham E, Stone MH, Farrar R et al. Quantitative analysis of wear and wear debris from metal-on-metal hip prostheses tested in a physiological hip joint simulator. Biomed Mater Eng 2001;11:143-157.

13 Sieber HP, Rieker CB, Kottig P. Analysis of 118 second-generation metal-on-metal retrieved hip implants. J Bone Joint Surg Br 1999;81:46-50.

14 Rieker C, Kottig P. In vivo tribological performance of 231 metal-on-metal hip articulations. HIP Int 2002;12:73-76.

15 Hallab NJ, Messina C, Skipor A, Jacobs JJ. Differences in the fretting corrosion of metal-metal and ceramic-metal modular junctions of total hip replacements. J Orthop Res 2004;22:250-259.

16 Doorn PF, Campbell PA, Worrall J, Benya PD, McKellop HA, Amstutz HC. Metal wear particle characterization from metal on metal total hip replacements: transmission electron microscopy study of periprosthetic tissues and isolated particles. J Biomed Mater Res 1998;42:103-111.

17 Catelas I, Medley JB, Campbell PA, Huk OL, Bobyn JD. Comparison of in vitro with in vivo characteristics of wear particles from metal-metal hip implants. J Biomed Mater Res B Appl Biomater 2004;70:167-178.

18 Keegan GM, Learmonth ID, Case CP. Orthopaedic metals and their potential toxicity in the arthroplasty patient: A REVIEW OF CURRENT KNOWLEDGE AND FUTURE STRATEGIES. J Bone Joint Surg Br 2007;89:567-573.

19 MacDonald SJ, McCalden RW, Chess DG, Bourne RB, Rorabeck CH, Cleland D et al. Metal-on-metal versus polyethylene in hip arthroplasty: a randomized clinical trial. Clin Orthop Relat Res 2003;282-296.

20 Gilbert JL, Zarka L, Chang E, Thomas CH. The reduction half cell in biomaterials corrosion: oxygen diffusion profiles near and cell response to polarized titanium surfaces. J Biomed Mater Res 1998;42:321-330.

21 Danscher G. In vivo liberation of gold ions from gold implants. Autometallographic tracing of gold in cells adjacent to metallic gold. Histochem Cell Biol 2002;117:447-452.

22 Larsen A, Stoltenberg M, Danscher G. In vitro liberation of charged gold atoms: autometallographic tracing of gold ions released by macrophages grown on metallic gold surfaces. Histochem Cell Biol 2007;128:1-6.

23 Mu Y, Kobayashi T, Sumita M, Yamamoto A, Hanawa T. Metal ion release from titanium with active oxygen species generated by rat macrophages in vitro. J Biomed Mater Res 2000;49:238-243.

24 Case CP, Langkamer VG, James C, Palmer MR, Kemp AJ, Heap PF et al. Widespread dissemination of metal debris from implants. J Bone Joint Surg Br 1994;76:701-712.

25 Timbrell J.A. Principles of biochemical toxicology. 4 ed. Taylor & Francis Ltd London 1982.

26 Jacobs JJ, Hallab NJ, Skipor AK, Urban RM. Metal degradation products: a cause for concern in metal-metal bearings? Clin Orthop Relat Res 2003;139-147.

27 Lewis CG, Sunderman FW, Jr. Metal carcinogenesis in total joint arthroplasty. Animal models. Clin Orthop Relat Res 1996;S264-S268.

28 Memoli VA, Urban RM, Alroy J, Galante JO. Malignant neoplasms associated with orthopedic implant materials in rats. J Orthop Res 1986;4:346-355.

29 Gillespie WJ, Frampton CM, Henderson RJ, Ryan PM. The incidence of cancer following total hip replacement. J Bone Joint Surg Br 1988;70:539-542.

30 Visuri T, Koskenvuo M. Cancer risk after Mckee-Farrar total hip replacement. Orthopedics 1991;14:137-142.

31 Signorello LB, Ye W, Fryzek JP, Lipworth L, Fraumeni JF, Jr., Blot WJ et al. Nationwide study of cancer risk among hip replacement patients in Sweden. J Natl Cancer Inst 2001;93:1405-1410.

32 Onega T, Baron J, MacKenzie T. Cancer after total joint arthroplasty: a meta-analysis. Cancer Epidemiol Biomarkers Prev 2006;15:1532-1537.

33 Hallab NJ, Anderson S, Caicedo M, Skipor A, Campbell P, Jacobs JJ. Immune responses correlate with serum-metal in metal-on-metal hip arthroplasty. J Arthroplasty 2004;19:88-93.

34 Hallab N, Merritt K, Jacobs JJ. Metal sensitivity in patients with orthopaedic implants. J Bone Joint Surg Am 2001;83-A:428-436.

35 Jacobs JJ, Hallab NJ. Loosening and osteolysis associated with metal-on-metal bearings: A local effect of metal hypersensitivity? J Bone Joint Surg Am 2006;88:1171-1172.

36 Hallab NJ, Anderson S, Stafford T, Glant T, Jacobs JJ. Lymphocyte responses in patients with total hip arthroplasty. J Orthop Res 2005;23:384-391.

37 Doorn PF, Mirra JM, Campbell PA, Amstutz HC. Tissue reaction to metal on metal total hip prostheses. Clin Orthop Relat Res 1996;S187-S205.

38 Langkamer VG, Case CP, Heap P, Taylor A, Collins C, Pearse M et al. Systemic distribution of wear debris after hip replacement. A cause for concern? J Bone Joint Surg Br 1992;74:831-839.

39 Urban RM, Jacobs JJ, Tomlinson MJ, Gavrilovic J, Black J, Peoc'h M. Dissemination of wear particles to the liver, spleen, and abdominal lymph nodes of patients with hip or knee replacement. J Bone Joint Surg Am 2000;82:457-476.

40 Shea KG, Lundeen GA, Bloebaum RD, Bachus KN, Zou L. Lymphoreticular dissemination of metal particles after primary joint replacements. Clin Orthop Relat Res 1997;219-226.

41 Brown C, Fisher J, Ingham E. Biological effects of clinically relevant wear particles from metal-on-metal hip prostheses. Proc Inst Mech Eng [H] 2006;220:355-369.

42 Catelas I, Petit A, Zukor DJ, Antoniou J, Huk OL. TNF-alpha secretion and macrophage mortality induced by cobalt and chromium ions in vitro-qualitative analysis of apoptosis. Biomaterials 2003;24:383-391.

43 Lee SH, Brennan FR, Jacobs JJ, Urban RM, Ragasa DR, Glant TT. Human monocyte/macrophage response to cobalt-chromium corrosion products and titanium particles in patients with total joint replacements. J Orthop Res 1997;15:40-49.

44 Haynes DR, Rogers SD, Hay S, Pearcy MJ, Howie DW. The differences in toxicity and release of bone-resorbing mediators induced by titanium and cobalt-chromium-alloy wear particles. J Bone Joint Surg Am 1993;75:825-834.

45 Trindade MC, Lind M, Sun D, Schurman DJ, Goodman SB, Smith RL. In vitro reaction to orthopaedic biomaterials by macrophages and lymphocytes isolated from patients undergoing revision surgery. Biomaterials 2001;22:253-259.

46 Horowitz SM, Luchetti WT, Gonzales JB, Ritchie CK. The effects of cobalt chromium upon macrophages. J Biomed Mater Res 1998;41:468-473.

47 Coen N, Kadhim MA, Wright EG, Case CP, Mothersill CE. Particulate debris from a titanium metal prosthesis induces genomic instability in primary human fibroblast cells. Br J Cancer 2003;88:548-552.

48 Doherty AT, Howell RT, Ellis LA, Bisbinas I, Learmonth ID, Newson R et al. Increased chromosome translocations and aneuploidy in peripheral blood lymphocytes of patients having revision arthroplasty of the hip. J Bone Joint Surg Br 2001;83:1075-1081.

49 Ziaee H, Daniel J, Datta AK, Blunt S, McMinn DJ. Transplacental transfer of cobalt and chromium in patients with metal-on-metal hip arthroplasty: a controlled study. J Bone Joint Surg Br 2007;89:301-305.

50 Davies AP, Sood A, Lewis AC, Newson R, Learmonth ID, Case CP. Metal-specific differences in levels of DNA damage caused by synovial fluid recovered at revision arthroplasty. J Bone Joint Surg Br 2005;87:1439-1444.

51 Ladon D, Doherty A, Newson R, Turner J, Bhamra M, Case CP. Changes in metal levels and chromosome aberrations in the peripheral blood of patients after metal-on-metal hip arthroplasty. J Arthroplasty 2004;19:78-83.

52 Roach P, Eglin D, Rohde K, Perry CC. Modern biomaterials: a review-bulk properties and implications of surface modifications. J Mater Sci Mater Med 2007;18:1263-1277.

53 Futami T, Fujii N, Ohnishi H, Taguchi N, Kusakari H, Ohshima H et al. Tissue response to titanium implants in the rat maxilla: ultrastructural and histochemical observations of the bone-titanium interface. J Periodontol 2000;71:287-298.

54 Sennerby L, Thomsen P, Ericson LE. Early tissue response to titanium implants inserted in rabbit cortical bone. Journal of Materials Science: Materials in Medicine 1993;4:494-502.

55 Walivaara B, Aronsson BO, Rodahl M, Lausmaa J, Tengvall P. Titanium with different oxides: in vitro studies of protein adsorption and contact activation. Biomaterials 1994;15:827-834.

56 Kao WJ, Hubbell JA, Anderson JM. Protein-mediated macrophage adhesion and activation on biomaterials: a model for modulating cell behavior. J Mater Sci Mater Med 1999;10:601-605.

57 Ziats NP, Miller KM, Anderson JM. In vitro and in vivo interactions of cells with biomaterials. Biomaterials 1988;9:5-13.

58 Buser D, Schenk RK, Steinemann S, Fiorellini JP, Fox CH, Stich H. Influence of surface characteristics on bone integration of titanium implants. A histomorphometric study in miniature pigs. J Biomed Mater Res 1991;25:889-902.

59 Chou L, Firth JD, Nathanson D, Uitto VJ, Brunette DM. Effects of titanium on transcriptional and post-transcriptional regulation of fibronectin in human fibroblasts. J Biomed Mater Res 1996;31:209-217.

60 Hunt JA, Flanagan BF, McLaughlin PJ, Strickland I, Williams DF. Effect of biomaterial surface charge on the inflammatory response: evaluation of cellular infiltration and TNF alpha production. J Biomed Mater Res 1996;31:139-144.

61 Crowninshield R. An overview of prosthetic materials for fixation. Clin Orthop Relat Res 1988;166-172.

62 Albrektsson T, Branemark PI, Hansson HA, Lindstrom J. Osseointegrated titanium implants. Requirements for ensuring a long-lasting, direct bone-to-implant anchorage in man. Acta Orthop Scand 1981;52:155-170.

63 Brunette DM, Chehroudi B. The effects of the surface topography of micromachined titanium substrata on cell behavior in vitro and in vivo. J Biomech Eng 1999;121:49-57.

64 Kieswetter K, Schwartz Z, Hummert TW, Cochran DL, Simpson J, Dean DD et al. Surface roughness modulates the local production of growth factors and cytokines by osteoblast-like MG-63 cells. J Biomed Mater Res 1996;32:55-63.

65 Pearson BS, Klebe RJ, Boyan BD, Moskowicz D. Comments on the clinical application of fibronectin in dentistry. J Dent Res 1988;67:515-517.

66 Refai AK, Textor M, Brunette DM, Waterfield JD. Effect of titanium surface topography on macrophage activation and secretion of proinflammatory cytokines and chemokines. J Biomed Mater Res A 2004;70:194-205.

67 Rostlund T, Thomsen P, Bjursten LM, Ericson LE. Difference in tissue response to nitrogen-ion-implanted titanium and c.p. titanium in the abdominal wall of the rat. J Biomed Mater Res 1990;24:847-860.

68 Johansson CB, Albrektsson T, Ericson LE, Thomsen P. A quantitative comparison of the cell response to commercially pure titanium and Ti-6Al-4V implants in the abdominal wall of rats. Journal of Materials Science: Materials in Medicine 1992;3:126-136.

69 Ingham E, Fisher J. The role of macrophages in osteolysis of total joint replacement. Biomaterials 2005;26:1271-1286.

70 Thomsen P, Gretzer C. Macrophage interactions with modified material surfaces. Current Opinion in Solid State and Materials Science 2001;5:163-176.

71 Bi Y, Collier TO, Goldberg VM, Anderson JM, Greenfield EM. Adherent endotoxin mediates biological responses of titanium particles without stimulating their phagocytosis. J Orthop Res 2002;20:696-703.

72 Fritz EA, Glant TT, Vermes C, Jacobs JJ, Roebuck KA. Chemokine gene activation in human bone marrow-derived osteoblasts following exposure to particulate wear debris. J Biomed Mater Res A 2006.

73 Nakashima Y, Sun DH, Trindade MC, Maloney WJ, Goodman SB, Schurman DJ et al. Signaling pathways for tumor necrosis factor-alpha and interleukin-6 expression in human macrophages exposed to titanium-alloy particulate debris in vitro. J Bone Joint Surg Am 1999;81:603-615.

74 Garrigues GE, Cho DR, Rubash HE, Goldring SR, Herndon JH, Shanbhag AS. Gene expression clustering using self-organizing maps: analysis of the macrophage response to particulate biomaterials. Biomaterials 2005;26:2933-2945.

75 Goodman S. Wear particulate and osteolysis. Orthop Clin North Am 2005;36:41-8, vi.

76 Wooley PH, Schwarz EM. Aseptic loosening. Gene Ther 2004;11:402-407.

77 Haynes DR, Crotti TN, Zreiqat H. Regulation of osteoclast activity in peri-implant tissues. Biomaterials 2004;25:4877-4885.

78 Schmidmaier G, Lucke M, Schwabe P, Raschke M, Haas NP, Wildemann B. Collective review: bioactive implants coated with poly(D,L-lactide) and growth factors IGF-I, TGF-beta1, or BMP-2 for stimulation of fracture healing. J Long Term Eff Med Implants 2006;16:61-69.

79 Wozney JM. The bone morphogenetic protein family: multifunctional cellular regulators in the embryo and adult. Eur J Oral Sci 1998;106 Suppl 1:160-166.

80 Bostrom MP, Asnis P. Transforming growth factor beta in fracture repair. Clin Orthop Relat Res 1998;S124-S131.

81 Moses HL, Serra R. Regulation of differentiation by TGF-beta. Curr Opin Genet Dev 1996;6:581-586.

82 Heine U, Munoz EF, Flanders KC, Ellingsworth LR, Lam HY, Thompson NL et al. Role of transforming growth factor-beta in the development of the mouse embryo. J Cell Biol 1987;105:2861-2876.

83 Udagawa N. Mechanisms involved in bone resorption. Biogerontology 2002;3:79-83.

84 Gillitzer R, Goebeler M. Chemokines in cutaneous wound healing. J Leukoc Biol 2001;69:513-521.

85 Sabokbar A, Kudo O, Athanasou NA. Two distinct cellular mechanisms of osteoclast formation and bone resorption in periprosthetic osteolysis. J Orthop Res 2003;21:73-80.

86 Lee SE, Chung WJ, Kwak HB, Chung CH, Kwack KB, Lee ZH et al. Tumor necrosis factor-alpha supports the survival of osteoclasts through the activation of Akt and ERK. J Biol Chem 2001;276:49343-49349.

87 Lam J, Takeshita S, Barker JE, Kanagawa O, Ross FP, Teitelbaum SL. TNF-alpha induces osteoclastogenesis by direct stimulation of macrophages exposed to permissive levels of RANK ligand. J Clin Invest 2000;106:1481-1488.

88 Fuller K, Murphy C, Kirstein B, Fox SW, Chambers TJ. TNFalpha potently activates osteoclasts, through a direct action independent of and strongly synergistic with RANKL. Endocrinology 2002;143:1108-1118.

89 Singer AJ, Clark RA. Cutaneous wound healing. N Engl J Med 1999;341:738-746.

90 Frost A, Jonsson KB, Nilsson O, Ljunggren O. Inflammatory cytokines regulate proliferation of cultured human osteoblasts. Acta Orthop Scand 1997;68:91-96.

91 Mundy GR. Role of cytokines in bone resorption. J Cell Biochem 1993;53:296-300.

92 Jilka RL, Hangoc G, Girasole G, Passeri G, Williams DC, Abrams JS et al. Increased osteoclast development after estrogen loss: mediation by interleukin-6. Science 1992;257:88-91.

93 Takeuchi T, Tsuboi T, Arai M, Togari A. Adrenergic stimulation of osteoclastogenesis mediated by expression of osteoclast differentiation factor in MC3T3-E1 osteoblast-like cells. Biochem Pharmacol 2001;61:579-586.

94 Goodman SB, Ma T, Chiu R, Ramachandran R, Smith RL. Effects of orthopaedic wear particles on osteoprogenitor cells. Biomaterials 2006;27:6096-6101.

95 Hadjidakis DJ, Androulakis II. Bone remodeling. Ann N Y Acad Sci 2006;1092:385-396.

96 Hofbauer LC, Lacey DL, Dunstan CR, Spelsberg TC, Riggs BL, Khosla S. Interleukin-1beta and tumor necrosis factor-alpha, but not interleukin-6, stimulate osteoprotegerin ligand gene expression in human osteoblastic cells. Bone 1999;25:255-259.

97 Kimble RB, Srivastava S, Ross FP, Matayoshi A, Pacifici R. Estrogen deficiency increases the ability of stromal cells to support murine osteoclastogenesis via an interleukin-1and tumor necrosis factor-mediated stimulation of macrophage colony-stimulating factor production. J Biol Chem 1996;271:28890-28897.

98 Boyce BF, Xing L. Biology of RANK, RANKL, and osteoprotegerin. Arthritis Res Ther 2007;9 Suppl 1:S1.

99 Hallab NJ, Anderson S, Caicedo M, Brasher A, Mikecz K, Jacobs JJ. Effects of soluble metals on human peri-implant cells. J Biomed Mater Res A 2005;74:124-140.

100 Huk OL, Catelas I, Mwale F, Antoniou J, Zukor DJ, Petit A. Induction of apoptosis and necrosis by metal ions in vitro. J Arthroplasty 2004;19:84-87.

101 Vermes C, Glant TT, Hallab NJ, Fritz EA, Roebuck KA, Jacobs JJ. The potential role of the osteoblast in the development of periprosthetic osteolysis: review of in vitro osteoblast responses to wear debris, corrosion products, and cytokines and growth factors. J Arthroplasty 2001;16:95-100.

102 Catelas I, Petit A, Vali H, Fragiskatos C, Meilleur R, Zukor DJ et al. Quantitative analysis of macrophage apoptosis vs. necrosis induced by cobalt and chromium ions in vitro. Biomaterials 2005;26:2441-2453.

103 Kemp K, Jensen FP, Møller JT, Hansen G. Multi-element Analyses of Human Liver and Pig Liver and Kidney. 1-10-1975. Danish Atomic Energy Commission, Research Establishment Risø.

104 Faul F, Erdfelder E, Lang AG, Buchner A. G*Power 3: a flexible statistical power analysis program for the social, behavioral, and biomedical sciences. Behav Res Methods 2007;39:175-191.

105 Kemp K, Danscher G. Multi-element analysis of the rat hippocampus by proton induced X-ray emission spectroscopy (phosphorus, sulphur, chlorine, potassium, calcium, iron, zinc, copper, lead, bromine, and rubidium). Histochemistry 1979;59:167-176.

106 Kemp K, Jensen FP, Moller JT, Gyrd-Hansen N. Multi-element analysis of biological tissue by proton-induced X-ray emission spectroscopy. Physics in Medicine and Biology 1975;20:834-838.

107 Jakobsen SS, Danscher G, Stoltenberg M, Larsen A, Bruun JM, Mygind T et al. Cobalt-chromium-molybdenum alloy causes metal accumulation and metallothionein up-regulation in rat liver and kidney. Basic Clin Pharmacol Toxicol 2007;101:441-446.

108 Pfaffl MW, Tichopad A, Prgomet C, Neuvians TP. Determination of stable housekeeping genes, differentially regulated target genes and sample integrity: BestKeeper--Excel-based tool using pair-wise correlations. Biotechnol Lett 2004;26:509-515.

109 Bockman RS. Prostaglandin production by human blood monocytes and mouse peritoneal macrophages: synthesis dependent on in vitro culture conditions. Prostaglandins 1981;21:9-31.

110 Catelas I, Petit A, Marchand R, Zukor DJ, Yahia L, Huk OL. Cytotoxicity and macrophage cytokine release induced by ceramic and polyethylene particles in vitro. J Bone Joint Surg Br 1999;81:516-521.

111 Horowitz SM, Doty SB, Lane JM, Burstein AH. Studies of the mechanism by which the mechanical failure of polymethylmethacrylate leads to bone resorption. J Bone Joint Surg Am 1993;75:802-813.

112 Takebe J, Ito S, Champagne CM, Cooper LF, Ishibashi K. Anodic oxidation and hydrothermal treatment of commercially pure titanium surfaces increases expression of bone morphogenetic protein-2 in the adherent macrophage cell line J774A.1. J Biomed Mater Res A 2006.

113 Jakobsen SS, Larsen A, Stoltenberg M, Bruun JM, Soballe K. Effects of as-cast and wrought Cobalt-Chrome-Molybdenum and Titanium-Aluminium-Vanadium alloys on cytokine gene expression and protein secretion in J774A.1 macrophages. Eur Cell Mater 2007;14:45-54.

114 Champagne CM, Takebe J, Offenbacher S, Cooper LF. Macrophage cell lines produce osteoinductive signals that include bone morphogenetic protein-2. Bone 2002;30:26-31.

115 Takebe J, Champagne CM, Offenbacher S, Ishibashi K, Cooper LF. Titanium surface topography alters cell shape and modulates bone morphogenetic protein 2 expression in the J774A.1 macrophage cell line. J Biomed Mater Res A 2003;64:207-216.

116 Zdolsek JM, Olsson GM, Brunk UT. Photooxidative damage to lysosomes of cultured macrophages by acridine orange. Photochem Photobiol 1990;51:67-76.

117 Fadeel B. Programmed cell clearance. Cell Mol Life Sci 2003;60:2575-2585.

118 Udupa G, Singaperumal M, Sirohi RS, Kothiyal MP. Characterization of surface topography by confocal microscopy: I. Principles and the measurement system. Measurement Science and Technology 2000;11:305-314.

119 Udupa G, Singaperumal M, Sirohi RS, Kothiyal MP. Characterization of surface topography by confocal microscopy: II. The micro and macro surface irregularities. Measurement Science and Technology 2000;11:315-329.

120 Ragab AA, Van De MR, Lavish SA, Goldberg VM, Ninomiya JT, Carlin CR et al. Measurement and removal of adherent endotoxin from titanium particles and implant surfaces. J Orthop Res 1999;17:803-809.

121 Xing Z, Pabst MJ, Hasty KA, Smith RA. Accumulation of LPS by polyethylene particles decreases bone attachment to implants. J Orthop Res 2006;24:959-966.

122 Greenfield EM, Bi Y, Ragab AA, Goldberg VM, Nalepka JL, Seabold JM. Does endotoxin contribute to aseptic loosening of orthopedic implants? J Biomed Mater Res B Appl Biomater 2005;72:179-185.

123 Tatro JM, Taki N, Islam AS, Goldberg VM, Rimnac CM, Doerschuk CM et al. The balance between endotoxin accumulation and clearance during particle-induced osteolysis in murine calvaria. J Orthop Res 2006.

124 Aerssens J, Boonen S, Lowet G, Dequeker J. Interspecies differences in bone composition, density, and quality: potential implications for in vivo bone research. Endocrinology 1998;139:663-670.

125 Soballe K. Hydroxyapatite ceramic coating for bone implant fixation. Mechanical and histological studies in dogs. Acta Orthop Scand Suppl 1993;255:1-58.

126 Linde F, Sorensen HC. The effect of different storage methods on the mechanical properties of trabecular bone. J Biomech 1993;26:1249-1252.

127 Overgaard S, Soballe K, Jorgen H, Gundersen G. Efficiency of systematic sampling in histomorphometric bone research illustrated by hydroxyapatite-coated implants: optimizing the stereological vertical-section design. J Orthop Res 2000;18:313-321.

128 Gotfredsen K, Budtz-Jorgensen E, Jensen LN. A method for preparing and staining histological sections containing titanium implants for light microscopy. Stain Technol 1989;64:121-127.

129 Karrholm J, Borssen B, Lowenhielm G, Snorrason F. Does early micromotion of femoral stem prostheses matter? 4-7-year stereoradiographic follow-up of 84 cemented prostheses. J Bone Joint Surg Br 1994;76:912-917.

130 Ryd L, Albrektsson BE, Carlsson L, Dansgard F, Herberts P, Lindstrand A et al. Roentgen stereophotogrammetric analysis as a predictor of mechanical loosening of knee prostheses. J Bone Joint Surg Br 1995;77:377-383.

131 Berzins A, Shah B, Weinans H, Sumner DR. Nondestructive measurements of implant-bone interface shear modulus and effects of implant geometry in pull-out tests. J Biomed Mater Res 1997;34:337-340.

132 Harrigan TP, Kareh J, Harris WH. The influence of support conditions in the loading fixture on failure mechanisms in the push-out test: a finite element study. J Orthop Res 1990;8:678-684.

133 Dhert WJ, Verheyen CC, Braak LH, de W, Jr., Klein CP, de GK et al. A finite element analysis of the push-out test: influence of test conditions. J Biomed Mater Res 1992;26:119-130.

134 Baddeley AJ, Gundersen HJ, Cruz-Orive LM. Estimation of surface area from vertical sections. J Microsc 1986;142:259-276.

135 Overgaard S. Calcium phosphate coatings for fixation of bone implants. Sweden: Faculty of Health Science, University of Aarhus, 2000.

136 Gundersen HJ, Bagger P, Bendtsen TF, Evans SM, Korbo L, Marcussen N et al. The new stereological tools: disector, fractionator, nucleator and point sampled intercepts and their use in pathological research and diagnosis. APMIS 1988;96:857-881.

137 Sumner DR, Bryan JM, Urban RM, Kuszak JR. Measuring the volume fraction of bone ingrowth: a comparison of three techniques. J Orthop Res 1990;8:448-452.

138 Danscher G. Localization of gold in biological tissue. A photochemical method for light and electronmicroscopy. Histochemistry 1981;71:81-88.

139 Danscher G. Light and electron microscopic localization of silver in biological tissue. Histochemistry 1981;71:177-186.

140 Sadauskas E, Wallin H, Stoltenberg M, Vogel U, Doering P, Larsen A et al. Kupffer cells are central in the removal of nanoparticles from the organism. Part Fibre Toxicol 2007;4:10.

141 Kraft CN, Burian B, Diedrich O, Gessmann J, Wimmer MA, Pennekamp PH. Microvascular response of striated muscle to common arthroplasty-alloys: A comparative in vivo study with CoCrMo, Ti-6Al-4V, and Ti-6Al-7Nb. J Biomed Mater Res A 2005;75:31-40.

142 Reuling N, Wisser W, Jung A, Denschlag HO. Release and detection of dental corrosion products in vivo: development of an experimental model in rabbits. J Biomed Mater Res 1990;24:979-991.

143 Stoltenberg M, Hogenhuis JA, Hauw JJ, Danscher G. Autometallographic tracing of bismuth in human brain autopsies. J Neuropathol Exp Neurol 2001;60:705-710.

144 Penkowa M. Metallothioneins are multipurpose neuroprotectants during brain pathology. FEBS J 2006;273:1857-1870.

145 Klaassen CD, Liu J, Choudhuri S. Metallothionein: an intracellular protein to protect against cadmium toxicity. Annu Rev Pharmacol Toxicol 1999;39:267-294.

146 Waalkes MP, Klaassen CD. Concentration of metallothionein in major organs of rats after administration of various metals. Fundam Appl Toxicol 1985;5:473-477.

147 Tohoyama H, Kadota H, Shiraishi E, Inouhe M, Joho M. Induction for the expression of yeast metallothionein gene, CUP1, by cobalt. Microbios 2001;104:99-104.

148 Kobayashi K, Kuroda J, Shibata N, Hasegawa T, Seko Y, Satoh M et al. Induction of metallothionein by manganese is completely dependent on interleukin-6 production. J Pharmacol Exp Ther 2007;320:721-727.

149 Sethi RK, Neavyn MJ, Rubash HE, Shanbhag AS. Macrophage response to cross-linked and conventional UHMWPE. Biomaterials 2003;24:2561-2573.

150 Bobyn JD, Pilliar RM, Cameron HU, Weatherly GC, Kent GM. The effect of porous surface configuration on the tensile strength of fixation of implants by bone ingrowth. Clin Orthop Relat Res 1980;291-298.

151 Murray DW, Rae T, Rushton N. The influence of the surface energy and roughness of implants on bone resorption. J Bone Joint Surg Br 1989;71:632-637.

152 Placko HE, Brown SA, Payer JH. Effects of microstructure on the corrosion behavior of CoCr porous coatings on orthopedic implants. J Biomed Mater Res 1998;39:292-299.

153 Lewis AC, Kilburn MR, Papageorgiou I, Allen GC, Case CP. Effect of synovial fluid, phosphate-buffered saline solution, and water on the dissolution and corrosion properties of CoCrMo alloys as used in orthopedic implants. J Biomed Mater Res A 2005;73:456-467.

154 Konttinen YT, Waris V, Xu JW, Jiranek WA, Sorsa T, Virtanen I et al. Transforming growth factor-beta 1 and 2 in the synovial-like interface membrane between implant and bone in loosening of total hip arthroplasty. J Rheumatol 1997;24:694-701.

155 Laquerriere P, Grandjean-Laquerriere A, Jallot E, Balossier G, Frayssinet P, Guenounou M. Importance of hydroxyapatite particles characteristics on cytokines production by human monocytes in vitro. Biomaterials 2003;24:2739-2747.

156 Grandjean-Laquerriere A, Laquerriere P, Guenounou M, Laurent-Maquin D, Phillips TM. Importance of the surface area ratio on cytokines production by human monocytes in vitro induced by various hydroxyapatite particles. Biomaterials 2005;26:2361-2369.

157 Hayakawa T, Yoshinari M, Nemoto K, Wolke JG, Jansen JA. Effect of surface roughness and calcium phosphate coating on the implant/bone response. Clin Oral Implants Res 2000;11:296-304.

158 Puleo DA, Holleran LA, Doremus RH, Bizios R. Osteoblast responses to orthopedic implant materials in vitro. J Biomed Mater Res 1991;25:711-723.

159 Jinno T, Goldberg VM, Davy D, Stevenson S. Osseointegration of surface-blasted implants made of titanium alloy and cobalt-chromium alloy in a rabbit intramedullary model. J Biomed Mater Res 1998;42:20-29.

160 Ahmad M, McCarthy MB, Gronowicz G. An in vitro model for mineralization of human osteoblast-like cells on implant materials. Biomaterials 1999;20:211-220.

161 Geesink RG. Osteoconductive coatings for total joint arthroplasty. Clin Orthop Relat Res 2002;53-65.